

Environmental Research Letters



LETTER

Permafrost-carbon mobilization in Beringia caused by deglacial meltwater runoff, sea-level rise and warming

OPEN ACCESS

RECEIVED

6 October 2018

REVISED

23 May 2019

ACCEPTED FOR PUBLICATION

3 June 2019

PUBLISHED

26 July 2019

Vera D Meyer^{1,2,3} , Jens Hefter¹ , Peter Köhler¹ , Ralf Tiedemann¹ , Rainer Gersonde¹,
Lukas Wacker⁴ and Gesine Mollenhauer^{1,2,3} ¹ Alfred-Wegener-Institute Helmholtz Zentrum für Polar- und Meeresforschung, D-27570 Bremerhaven, Germany² Department of Geosciences, University of Bremen, D-28359 Bremen, Germany³ MARUM—Center for Marine Environmental Science, D-28359 Bremen, Germany⁴ Department of Physics, Laboratory for Ion Beam Physics ETH Zürich 8093 Zürich, SwitzerlandE-mail: vera.meyer@awi.de

Original content from this work may be used under the terms of the [Creative Commons Attribution 3.0 licence](https://creativecommons.org/licenses/by/3.0/).

Any further distribution of this work must maintain attribution to the author(s) and the title of the work, journal citation and DOI.

**Keywords:** deglaciation, permafrost decomposition, Beringia, Bering Sea, biomarker, atmospheric CO₂, Northwest PacificSupplementary material for this article is available [online](#)**Abstract**

During the last deglaciation (18–8 kyr BP), shelf flooding and warming presumably led to a large-scale decomposition of permafrost soils in the mid-to-high latitudes of the Northern Hemisphere. Microbial degradation of old organic matter released from the decomposing permafrost potentially contributed to the deglacial rise in atmospheric CO₂ and also to the declining atmospheric radiocarbon contents ($\Delta^{14}\text{C}$). The significance of permafrost for the atmospheric carbon pool is not well understood as the timing of the carbon activation is poorly constrained by proxy data. Here, we trace the mobilization of organic matter from permafrost in the Pacific sector of Beringia over the last 22 kyr using mass-accumulation rates and radiocarbon signatures of terrigenous biomarkers in four sediment cores from the Bering Sea and the Northwest Pacific. We find that pronounced reworking and thus the vulnerability of old organic carbon to remineralization commenced during the early deglaciation (~16.8 kyr BP) when meltwater runoff in the Yukon River intensified riverbank erosion of permafrost soils and fluvial discharge. Regional deglaciation in Alaska additionally mobilized significant fractions of fossil, petrogenic organic matter at this time. Permafrost decomposition across Beringia's Pacific sector occurred in two major pulses that match the Bølling-Allerød and Preboreal warm spells and rapidly initiated within centuries. The carbon mobilization likely resulted from massive shelf flooding during meltwater pulses 1A (~14.6 kyr BP) and 1B (~11.5 kyr BP) followed by permafrost thaw in the hinterland. Our findings emphasize that coastal erosion was a major control to rapidly mobilize permafrost carbon along Beringia's Pacific coast at ~14.6 and ~11.5 kyr BP implying that shelf flooding in Beringia may partly explain the centennial-scale rises in atmospheric CO₂ at these times. Around 16.5 kyr BP, the mobilization of old terrigenous organic matter caused by meltwater-floods may have additionally contributed to increasing CO₂ levels.

1. Introduction

Circumarctic permafrost soils preserve large quantities of organic matter and presently store twice as much carbon as the atmosphere (Hugelius *et al* 2014, Strauss *et al* 2017). Future Arctic warming and sea-level rise are expected to induce widespread permafrost thaw and massive erosion of permafrost along arctic coastlines allowing for microbial degradation of

the presently freeze-locked organic matter (Vonk *et al* 2012, Strauss *et al* 2017). As a consequence, large quantities of greenhouse gases (CO₂ and CH₄) may be emitted into the atmosphere thereby amplifying global warming in a positive feedback (Koven *et al* 2011, Schuur *et al* 2015, Kleinen and Brovkin 2018). Projections of the magnitude and time-scales of future greenhouse-gas emissions related to permafrost degradation are highly uncertain as the pathways of carbon

in changing permafrost landscapes are insufficiently understood (Schuur *et al* 2015).

Investigating the role of permafrost decomposition for the atmospheric carbon pool during past episodes of climate change helps to better constrain the projected permafrost feedback during the 21st century and beyond.

During the last deglaciation (8–18 kyr BP) atmospheric CO₂ concentrations rose by ~90 ppm (Marcott *et al* 2014) while atmospheric $\Delta^{14}\text{C}$ concurrently declined by ~400‰ (Reimer *et al* 2013). Large parts of these changes occurred in three sudden steps (at 16.5, 14.6, and 11.5 kyr BP), during which CO₂ rose by 10–15 ppm within 100–200 years (Marcott *et al* 2014). Emissions of old CO₂ resulting from a combination of different dominantly marine processes are thought to have driven these deglacial atmospheric changes (e.g. Köhler *et al* 2005, Brovkin *et al* 2012). For the three sudden events, the carbon isotopic composition (¹³C and ¹⁴C) of atmospheric CO₂ suggests a significant contribution from old terrestrial carbon (Köhler *et al* 2014, Bauska *et al* 2016). Since the permafrost extent shrank by ~50 % over the deglaciation (Lindgren *et al* 2015)—likely caused by coastal erosion during sea-level rise and permafrost thaw due to warming—the resulting mobilization of old, permafrost carbon is considered the major component of the terrestrial contribution (Ciais *et al* 2012, Köhler *et al* 2014, Crichton *et al* 2016). Yet, the impact of permafrost on the atmospheric carbon is poorly resolved (Lindgren *et al* 2018). Most studies investigating the contributions of terrestrial carbon to the atmospheric changes are indirect, as they rely on interpreting atmospheric records with carbon-cycle models (Köhler *et al* 2014, Bauska *et al* 2016, Crichton *et al* 2016). However, the assumed timing of carbon release from degrading permafrost is very poorly constrained by proxy data as deglacial records of carbon mobilization are very sparse (Tesi *et al* 2016, Winterfeld *et al* 2018, Martens *et al* 2019).

Biomarker records from the Laptev, Chukchi and Okhotsk Seas provide evidence for rapid thaw-induced mobilization of permafrost carbon and subsequent river discharge (Tesi *et al* 2016) as well as for coastal erosion of permafrost associated with rapid sea-level rise (Winterfeld *et al* 2018, Martens *et al* 2019).

Experiments with carbon-cycle models suggest that flooding of the extensive East Siberian Arctic, Chukchi and Bering Shelves during melt-water pulses 1A and 1B (mwp-A1, mwp-1B) may have substantially contributed to the centennial-scale rises in CO₂ at 14.6 and 11.5 kyr BP (Köhler *et al* 2014, Winterfeld *et al* 2018). Hence, a key region to understand the deglacial permafrost-carbon feedback is Beringia, the area stretching from the Lena River in Siberia to the Mackenzie River in Alaska (figure 1). During the last glacial, when sea-level low stands exposed the East Siberian Arctic, Bering and Chukchi Shelves, the Bering Land Bridge connected Alaska and Siberia (figure 1) to form

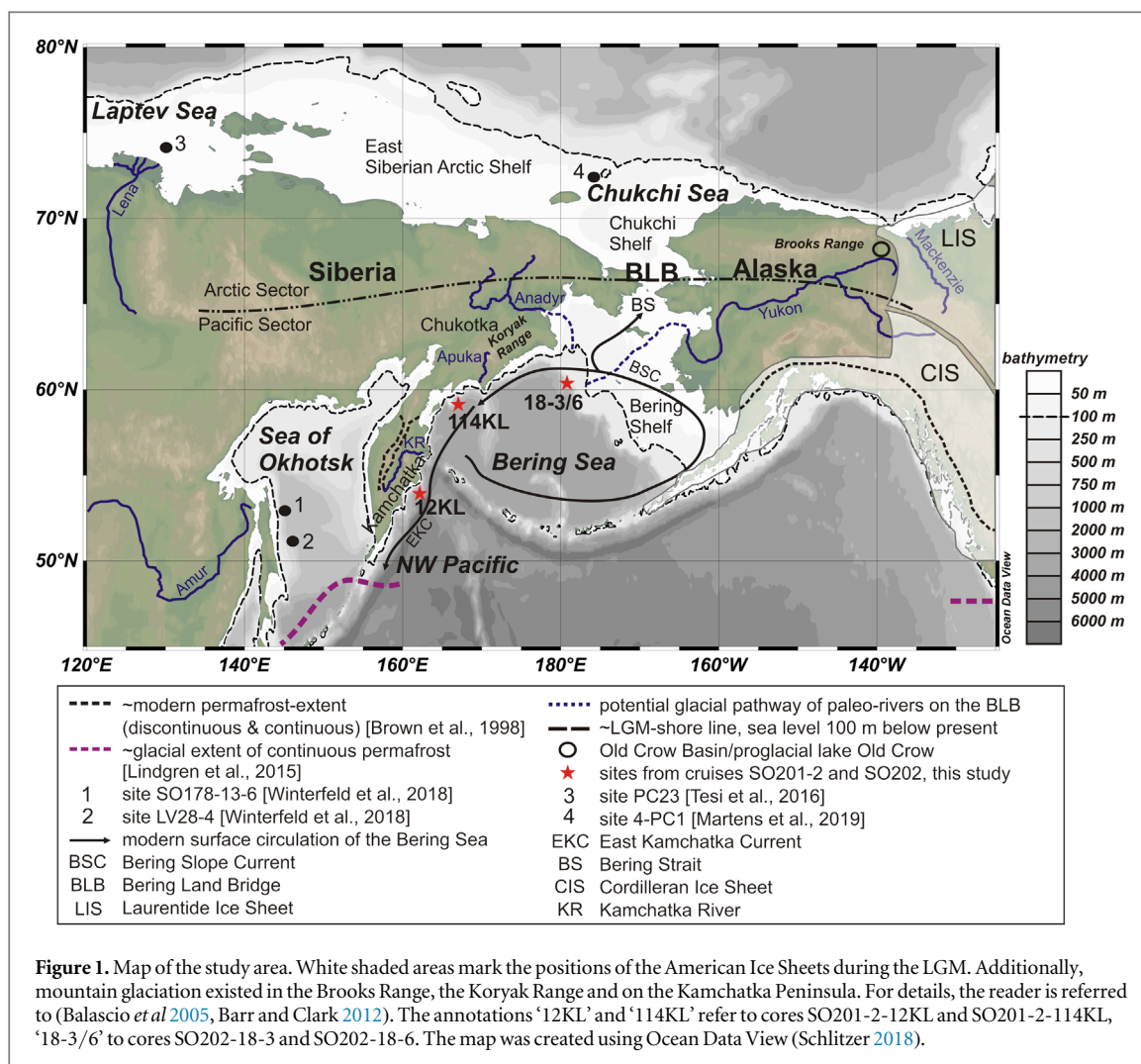
an extensive, largely unglaciated land mass (Balascio *et al* 2005, Barr and Clark 2012) where thick, carbon rich deposits (Yedoma) accumulated over the late Pleistocene (Strauss *et al* 2017). During the last glacial maximum (LGM), continuous permafrost extended from Siberia (including the Kamchatka Peninsula) over the Bering Land Bridge to Alaska (Lindgren *et al* 2015). Over the deglaciation continuous permafrost became discontinuous and sporadic over wide areas in Alaska and completely disappeared from the Bering Land Bridge and the lowlands in Kamchatka (Brown *et al* 1998, Lindgren *et al* 2015). As such, Beringia may have been relevant for both, the sea-level associated component of the deglacial permafrost feedback (Köhler *et al* 2014, Winterfeld *et al* 2018) and greenhouse-gas emissions related to inland permafrost thaw induced by warming. So far, evidence has been obtained for massive remobilization of permafrost carbon from the Lena River catchment (at 11.5 kyr BP) (Tesi *et al* 2016) as well as from the East Siberian Arctic and Chukchi Shelves (after ~9.5 and around ~13 kyr BP) (Keskitalo *et al* 2017, Martens *et al* 2019).

Yet, the timing of carbon mobilization from degrading permafrost in this region still remains elusive since existing records do not reach beyond ~13 kyr BP (Tesi *et al* 2016, Keskitalo *et al* 2017, Martens *et al* 2019) and some are not continuous (Keskitalo *et al* 2017, Martens *et al* 2019).

Here, we trace permafrost erosion in Beringia's Pacific sector (figure 1) since the LGM by analyzing terrigenous biomarkers and their radiocarbon signature in three marine sediment cores from the Bering Sea (cores SO202-18-3, SO202-18-6 and SO201-2-114KL, figure 1) and one from the subarctic Northwest Pacific (core SO201-2-12KL, figure 1). The catchments of these cores comprise the drainage basins of the Yukon and paleo-Anadyr Rivers (i.e. Alaska, the Bering Land Bridge and Chukotka (cores SO202-18-3/SO202-18-6)), the southern flanks of the Koryak Range and adjacent lowlands, drained by the small Apuka River in Siberia (core SO201-2-114KL), and the Kamchatka Peninsula drained by the Kamchatka River (core SO201-2-12KL).

2. Scientific approach

Degradation of permafrost is accompanied by various complex processes comprising destabilization of hillslopes, lake shores and riverbanks (including large thaw slumps), active-layer deepening, development of thermokarst lakes and wetlands as well as intensified overland drainage (e.g. Vonk and Gustafsson 2013). As a consequence, fluvial transport of permafrost-derived particulate organic matter amplifies. Moreover, rising sea-level and warming can induce massive destruction of permafrost along coastlines by physical erosion and thermal collapse of coastal bluffs (Vonk *et al* 2012, Jones *et al* 2018). Together these



processes increase the deposition rates of permafrost carbon in marine sediments (Vonk and Gustafsson 2013). At the same time, remineralization of the unlocked organic carbon takes place in thawed soils, lakes, during riverine transport, in the marine water column and during cross-shelf transport prior to final burial (Gustafsson *et al* 2011, Vonk *et al* 2012, 2014, Bröder *et al* 2018). Terrigenous biomarkers deposited in marine sediments are usually older than the respective deposition age due to intermediate storage in terrestrial reservoirs (e.g. soils) or the duration of transport processes prior to final burial (Kusch *et al* 2010, Bröder *et al* 2018). The so-called pre-depositional ages describe the age of terrigenous biomarkers at the time of deposition (Winterfeld *et al* 2018) providing an estimate on the time-scales of those reservoir effects. Due to the long preservation in frozen soils, permafrost-derived organic matter found in marine sediments is identifiable by high pre-depositional ages (Vonk *et al* 2012, Winterfeld *et al* 2018). Thus, mass accumulation rates combined with pre-depositional ages of terrigenous biomarkers in marine sediments are qualitative proxies of past permafrost decomposition and indicate the vulnerability of

permafrost carbon to remineralization (Tesi *et al* 2016, Winterfeld *et al* 2018).

In order to reconstruct the timing of deglacial permafrost retreat in Beringia we determine the mass accumulation rates of high molecular weight *n*-alkanoic acids (hereafter referred to as fatty acids) and high molecular weight *n*-alkanes (hereafter referred to as alkanes), both constituents of epicuticular wax layers (leaf wax lipids) of higher land plants (Eglinton and Hamilton 1967). Additionally, branched glycerol dialkyl glycerol tetraethers (brGDGTs) are quantified. BrGDGTs are bacterial biomarkers and in coastal marine sediments serve as indicator for input of soil and riverine organic matter (Hopmans *et al* 2004, DeJonge *et al* 2015). Compound-specific radiocarbon analysis of fatty acids and alkanes is performed to determine pre-depositional ages (Winterfeld *et al* 2018). The P_{aq} (Ficken *et al* 2000), a proxy of the relative contribution of aquatic to terrestrial plants, is applied to trace wetland development in the hinterland as this is a characteristic feature of degrading permafrost landscapes (AMAP 2012, Lindgren *et al* 2018). Existing records on thermokarst lake expansion (Walter Anthony *et al* 2014) are used as indicators of thaw-induced processes in the hinterland.

Since the Yukon-River catchment holds various fossil, thermally degraded (mature) deposits (e.g. coal or oil shales, e.g. Alaska State Office 2009), ^{14}C -depleted organic matter eroded from those ancient deposits is a potential source of old terrigenous biomarkers next to thermally immature Yedoma. In order to distinguish between contributions of petrogenic and Yedoma-derived carbon we analyze the fractional abundances of homohopane isomers—bacterial biomarkers—($f\beta\beta$, see supplementary material available online at stacks.iop.org/ERL/14/085003/mmedia) which can be used as indicator of thermal maturity of organic matter in the geological record (e.g. Farrimond *et al* 1998). The $f\beta\beta$ is combined with the carbon preference indices of alkanes and fatty acids (CPI_{alk} ; CPI_{FA}) which are also common indicators of degradation and thermal maturity (Bray and Evans 1961, Kvenvolden 1966). For more analytical details including core chronologies, the reader is referred to the supplementary material.

3. Results and discussion

3.1. The LGM (23–19 kyr BP)

Pre-depositional ages of the alkanes and fatty acids deposited during the LGM at the three core location are $>16\,000$ years (figures 2(i)–(k), table 1). Nowadays, leaf-wax lipids found off Arctic drainage basins underlain by continuous permafrost as well as lipids deposited off Siberian coastlines that currently undergo massive erosion are several thousand years old due to substantial contributions of ancient organic matter from Yedoma (~ 5500 – $\sim 13\,000$ years; Lena, Kolyma, Indigirka Rivers (Feng *et al* 2013, Gustafsson *et al* 2011); up to $\sim 18\,000$ years off eroded coasts (Vonk *et al* 2014)). By contrast, lipids deposited off permafrost-free catchments are much younger (~ 900 – 4400 years) (Kusch *et al* 2010). Thus, the relatively high LGM pre-depositional ages in our cores may indicate large proportions of old organic carbon from ancient Yedoma. This interpretation is in line with relatively high values in $f\beta\beta$, CPI_{alk} and CPI_{FA} (figures 3(b), (d) and (h)) which render old but little degraded organic matter the dominant source for the alkanes and fatty acids at this time. Our CPI_{alk} and CPI_{FA} values (~ 4 – 8) are in the range of CPI-values reported in Siberian and Alaskan Yedoma deposits (3–13) (Sánchez-García *et al* 2014, Jongejans *et al* 2018).

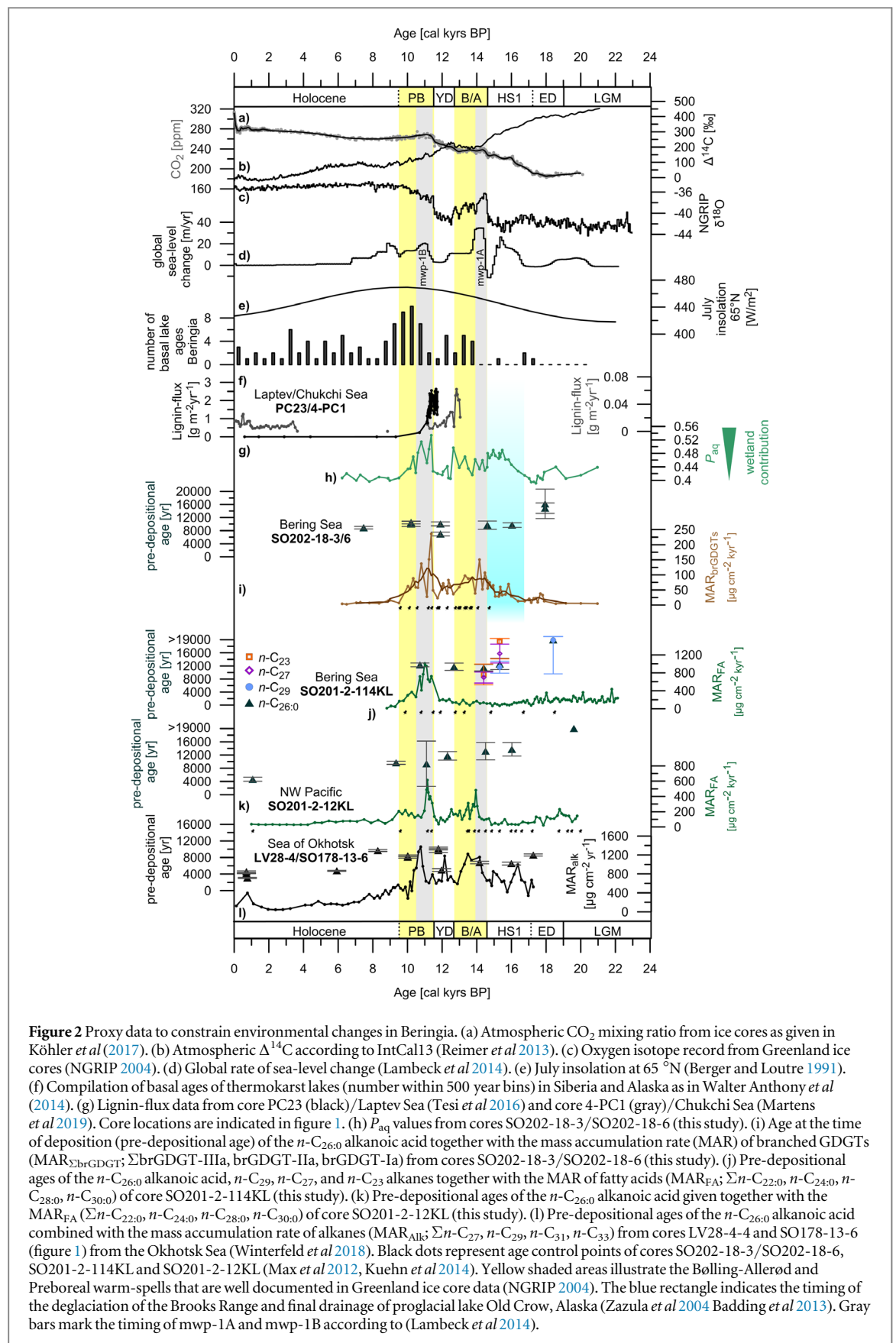
Minimal mass accumulation rates of terrigenous biomarkers at all sites (figures 2(i)–(k)) point to relatively little coastal erosion and fluvial discharge of permafrost carbon during the LGM. This is in line with the presence of intact continuous permafrost in Beringia (Lindgren *et al* 2015), cold sea surface temperatures (SST) in the subarctic North Pacific (Meyer *et al* 2016, Méheust *et al* 2018, Maier *et al* 2018) and a continental climate with very cold winters (Elias 2001, Anderson and Lozhkin 2015).

3.2. The early deglaciation (19–15 kyr BP)

The early deglaciation is characterized by dissimilar patterns in mass accumulation rates of the different biomarkers. All cores record enhanced burial of old alkanes (pre-depositional age: $>11\,600$ years) between ~ 16.8 and 15 kyr BP coincident with Heinrich Stadial 1 (figures 2(i)–(k), 3(b), (d) and (h)). Off the Bering Shelf (cores SO202-18-3/SO202-18-6) this increase is accompanied by enhanced burial of old fatty acids (pre-depositional age: >9600 years) and brGDGT while off the Apuka River (core SO201-2-114KL) and Kamchatka (core SO201-2-12KL) the fatty acids do not follow the increase reported in the alkanes but remain constant until ~ 14.6 kyr BP (figures 2(i)–(k), 3(a), (d) and (g)). Distinct minima in CPI_{alk} (~ 3 – 4) occur concurrently with the enhanced accumulation of alkanes at all sites (figures 3(b), (e) and (h)). These minima indicate that the amplification of alkane export is associated with a drastic increase in the degree of degradation of the alkanes. By contrast, all cores display constant CPI_{FA} -values across the LGM and early deglaciation (figures 3(b), (e) and (h)) indicating that the degradation state of the fatty acids remains unaltered. These discrepancies in mass-accumulation rates and CPI-values of alkanes and fatty acids imply that the compounds derive from different sources and record different erosion and transport processes.

Possible explanations for the lowering of CPI_{alk} include biogeochemical degradation of alkanes during land-ocean transport (e.g. Bröder *et al* 2016), changes in the composition of the vegetation (Bush and McInerney 2013), or contributions of petrogenic organic matter (Bray and Evans 1961). At all cores, the minima in CPI_{alk} are congruent with pronounced minima in $f\beta\beta$ which decreases by 0.3–0.6 units reaching values as low as 0.2–0.4 (figures 3(c), (f) and (i)). These minima in $f\beta\beta$ hint at massive reworking of petrogenic organic matter since the lowering of $f\beta\beta$ stems from a distinct increase in the diagenetic $\text{C}_{31}\alpha\beta\text{S}$ and $\text{C}_{31}\alpha\beta\text{R}$ epimers (figure S1) which form under elevated temperatures during burial (van Duin *et al* 1997, Farrimond *et al* 1998) and dominate over the biogenic $\text{C}_{31}\beta\beta\text{R}$ isomer in our cores (figure S1). Given the coincidence of the minima in CPI_{alk} and $f\beta\beta$ it is most likely that the low CPI_{alk} results from significant contributions of petrogenic alkanes. As the CPI_{alk} values (3–4) still exceed the characteristic value of petrogenic organic matter (~ 1) (Bray and Evans 1961), the old alkanes (pre-depositional age of 11 600–19 400 years) deposited at the core locations during the early deglaciation probably derive from a mixture of fossil petrogenic organic matter and old but less degraded material, most likely derived from Yedoma.

In contrast to the alkanes, the source of the fatty acids likely did not change significantly after the LGM considering that the CPI_{FA} is relatively constant across the LGM and the early deglaciation. The high pre-depositional ages of the fatty acids (9600–13 700 years, figures 2(i)–(k)) point to Yedoma deposits as the



predominant source, during the LGM as well as the early deglaciation.

As such, the concurrent increase in fatty acids and brGDGT off the Bering Shelf (cores SO202-18-3/

SO202-18-6; figures 2(i)–(k) and 3(a)) points to an initial destabilization of permafrost soils and subsequent organic matter remobilization in Alaska and on the Bering Land Bridge. By contrast, low

Table 1. Compound-specific radiocarbon data of terrigenous biomarkers, i.e. fatty acids (n -C_{26,0} alkanic acid) and n -alkanes (n -C₂₃, n -C₂₇ and n -C₂₉ alkanes) from cores SO202-18-6, SO202-18-3, SO201-2-114KL and SO201-2-12KL obtained by accelerator mass spectrometry (AMS).

| Sample depth (cm) | Deposition age (mid-point) (cal kyr BP) | Compound | Corrected F ¹⁴ C ± 1σ ^a | Δ ¹⁴ C ± 1σ (‰) ^a | Pre-depositional age ± 1σ (cal years) |
|------------------------|---|------------------------|---|---|---------------------------------------|
| SO202-18-6 | | | | | |
| 55-57 | 7.47 | n -C _{26,0} | 0.1882 ± 0.0068 | -813 ± 7 | 8900 ± 400 |
| 200-202 ^b | 10.21 | n -C _{26,0} | 0.1208 ± 0.0055 | -880 ± 5 | 10 450 ± 450 |
| 200-202 ^b | 10.21 | n -C _{26,0} | 0.1287 ± 0.0100 | -872 ± 10 | 10 050 ± 770 |
| 460-462 ^b | 11.90 | n -C _{26,0} | 0.1075 ± 0.0059 | -893 ± 6 | 10 050 ± 610 |
| 460-462 ^b | 11.90 | n -C _{26,0} | 0.1493 ± 0.0104 | -852 ± 10 | 6960 ± 600 |
| SO202-18-3 | | | | | |
| 739-742 | 14.60 | n -C _{26,0} | 0.0857 ± 0.0106 | -915 ± 11 | 9670 ± 1200 |
| 995-997 | 16.03 | n -C _{26,0} | 0.0730 ± 0.0051 | -928 ± 5 | 9630 ± 680 |
| 1146-1149 ^b | 17.94 | n -C _{26,0} | 0.0305 ± 0.0065 | -970 ± 6 | 14 850 ± 1600 |
| 1146-1149 ^b | 17.94 | n -C _{26,0} | 0.0282 ± 0.0136 | -972 ± 14 | 16 150 ± 4500 |
| SO201-2-114KL | | | | | |
| 39-41.5 | 10.72 | n -C _{26,0} | 0.0925 ± 0.0053 | -908 ± 5 | 12 300 ± 560 |
| 101-103.5 | 12.69 | n -C _{26,0} | 0.0792 ± 0.0091 | -921 ± 9 | 11 700 ± 1100 |
| 144-146.5 | 14.40 | n -C _{26,0} | 0.0686 ± 0.0080 | -932 ± 8 | 11 400 ± 1000 |
| 144-146.5 | 14.40 | n -C ₂₇ | 0.1006 ± 0.0173 | -900 ± 17 | 8450 ± 1600 |
| 144-146.5 | 14.40 | n -C ₂₃ | 0.0968 ± 0.0320 | -904 ± 32 | 9390 ± 3100 |
| 174-176.5 | 15.33 | n -C _{26,0} | 0.0506 ± 0.0105 | -950 ± 10 | 12 600 ± 1700 |
| 174-176.5 | 15.33 | n -C ₂₉ | 0.0669 ± 0.0148 | -934 ± 15 | 11 600 ± 1800 |
| 174-176.5 | 15.33 | n -C ₂₇ | 0.0396 ± 0.0131 | -961 ± 13 | 15 750 ± 2900 |
| 174-176.5 | 15.33 | n -C ₂₃ | 0.0276 ± 0.0150 | -973 ± 15 | 19 400 ± 5200 |
| 301-303.5 | 18.41 | n -C _{26,0} | <0.0164 | <-985 | >18 000 |
| 301-303.5 | 18.41 | n -C ₂₉ | 0.0229 ± 0.0198 | -977 ± 20 | 19 800 ± 10 300 |
| 301-303.5 | 18.41 | n -C ₂₇ | <0.0480 | <-952 | >9000 |
| 301-303.5 | 18.41 | n -C ₂₃ | <0.1095 | <-891 | >3000 |
| SO201-2-12KL | | | | | |
| 1-4.5 | 1.07 | n -C _{26,0} | 0.5389 ± 0.0350 | -465 ± 35 | 4660 ± 630 |
| 203-205 | 9.22 | n -C _{26,0} | 0.1405 ± 0.0074 | -861 ± 7 | 9640 ± 470 |
| 295-297 | 11.08 | n -C _{26,0} | 0.1149 ± 0.0736 | -886 ± 74 | 9340 ± 6800 |
| 419-422 | 12.30 | n -C _{26,0} | 0.0830 ± 0.0105 | -918 ± 10 | 11 700 ± 1200 |
| 609-612 | 14.43 | n -C _{26,0} | 0.0536 ± 0.0171 | -947 ± 17 | 13 100 ± 2600 |
| 693-696 | 15.90 | n -C _{26,0} | 0.0410 ± 0.0110 | -959 ± 11 | 13 700 ± 2000 |
| 896-898 | 19.82 | n -C _{26,0} | <0.0357 | <-965 | >19 000 |

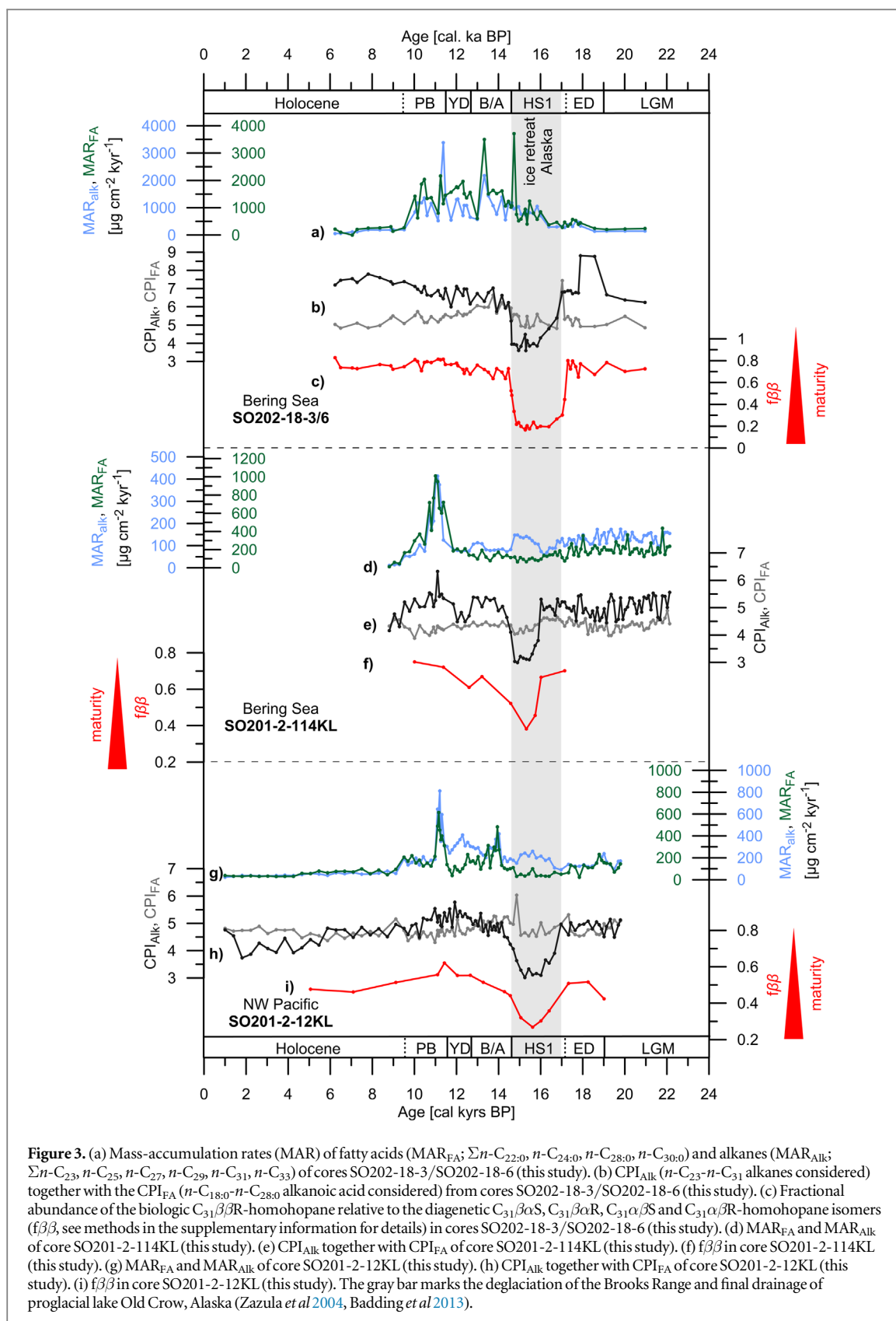
^a Corrected for procedure blanks, i.e. contaminating carbon introduced during sample processing, (fatty acids and alkanes) and for methylation (fatty acids only). For methodological details, see supplementary material. The AMS raw data are presented in table S1.

^b Split up for vacuum-line handling in order to keep the sample size (i.e. gas volume) appropriate for the AMS measurements. ^a 70%-split, ^b 30%-split.

export-rates of old fatty acids from the Apuka catchment and Kamchatka (cores SO201-2-114KL and SO201-2-12KL) indicate that permafrost likely remained stable in these regions throughout the early deglaciation until ~14.6 kyr BP (figures 2(j) and (k)).

The onset of increased accumulation of old terrigenous biomarkers off the Bering Shelf (cores SO202-18-3/SO202-18-6; figures 2(i) and 3(a)) between ~16.8 and 15 kyr BP coincides with the beginning retreat of the Cordilleran and Laurentide ice sheets and Alaskan mountain glaciers at ~19–16 kyr BP (Dyke 2004, Badding *et al* 2013, Maier *et al* 2018). A related massive meltwater input into the Yukon River system (Duk-Rodkin and Hughes 1994, Kennedy *et al* 2010), might have caused severe riverbank erosion of the organic-rich

Yedoma deposits in Alaska and on the Bering Land Bridge, subsequently enhancing the accumulation of permafrost-derived organic matter off the Bering Shelf (cores SO202-18-3/SO202-18-6). Also, the enhanced burial of petrogenic carbon at all sites matches the deglaciation of the Brooks Range and the final drainage of the proglacial Lake Old Crow (~16.8–15 kyr BP; figures 1 and 3) (Zazula *et al* 2004, Badding *et al* 2013). As mature deposits have been found at both locations (Barnes 1967, Alaska State Office 2009), it is likely that the massive reworking of petrogenic carbon is associated with these local deglaciation events in Alaska. The simultaneous deposition of petrogenic carbon along the core transect (figures 3(b), (e) and (h)) suggests that the petrogenic fraction of the Yukon load spilled out into the Northwest



Pacific, and was likely transported by the counter-clockwise surface circulation of the Bering Sea (figure 1). A profound influence from the Yukon load on the fatty acids deposited off the Apuka catchment and Kamchatka (cores SO201-2-114KL and SO201-2-12KL) seems unlikely considering that cores SO201-2-114KL

and SO201-2-12KL display a different pattern in mass accumulation rates of fatty acids than cores SO202-18-3/SO202-18-6 (figures 2(i)–(k) and 3(a)).

The increased accumulation of fatty acids and brGDGTs off the Bering Shelf (cores SO202-18-3/SO202-18-6) is also synchronous with a first

maximum in the global rate of sea-level rise (Lambeck *et al* 2014) (figure 2). The synchrony implies that rapid sea-level rise may have eroded permafrost deposits on the Bering Shelf during this interval (figures 2(d) and (i)).

Thawing of permafrost in the hinterland (Lindgren *et al* 2018) would be another mechanism increasing the fluvial export of old permafrost carbon from the Yukon and Anadyr drainage basins by active layer deepening, thaw-slumps along riverbanks and intensified overland drainage. This view is in line with rising summer insolation (figure 2(d)) (Berger and Loutre 1991) and air temperature in some parts of interior Alaska at this time (Kurek *et al* 2009). However, cold SST in the Bering Sea and the North Pacific (Meyer *et al* 2016, Méheust *et al* 2018) suggest that at least in Pacific Beringia (i.e. the Apuka catchment, Kamchatka, and the southern Bering Land Bridge) low air temperatures may have prevented permafrost from thawing. This is corroborated by the low mass accumulation rates of the fatty acids off the Apuka River mouth and Kamchatka (cores SO201-2-114KL and SO201-2-12KL, figures 2(j) and (k)). Since only very few Beringian thaw lakes date back to the early deglaciation (Walter *et al* 2007, Walter Anthony *et al* 2014) (figure 2(f)), thermokarst processes were probably limited in Siberia and Alaska pointing to mostly intact permafrost conditions across Beringia. P_{aq} shows a first maximum in wetland expansion at that time (figure 2(h)) congruent with the intensification of organic matter accumulation off the Bering Shelf (cores SO202-18-3/SO202-18-6; figure 2(i)). This may hint towards beginning ecosystem changes in the permafrost landscape of central/eastern Beringia associated with wetter conditions possibly due to the massive meltwater floods. However, in light of the substantial petrogenic contributions to the alkanes at that time, the P_{aq} —which is built on the relative abundance of alkane homologs (see supplementary material)—probably reflects altered relative abundances of alkane homologs that are associated with the petrogenic portion rather than with changing vegetation. Thus, widespread permafrost decomposition and thaw-induced riverine transport of permafrost carbon during the early deglaciation seem unlikely.

3.3. The late deglaciation (15–9 kyr BP)

Around ~15 kyr BP prominent increases in $f\beta\beta$ and CPI_{alk} (figures 3(b), (c), (e), (f), (h) and (i)) mark the cessation of major petrogenic contributions at all sites. Relatively high values in $f\beta\beta$, CPI_{alk} , CPI_{FA} throughout the late deglaciation and the Holocene (figures 3(b), (c), (e), (f), (h) and (i)) together with high pre-depositional ages (9600–12 300 years; figures 2(i)–(k); table 1) suggest that alkanes and fatty acids dominantly derive from old but less degraded deposits, most likely permafrost soils.

Our records display two major intervals of the enhanced inflow of permafrost carbon, that are

consistent with the Bølling-Allerød and Preboreal interstadials (figures 2(c), (i)–(k)). Both intervals are found in mass accumulation rates of terrestrial biomarkers off the Bering Shelf (cores SO202-18-3/SO202-18-6) and off Kamchatka (site SO201-2-12KL), while in core SO201-2-114KL only one peak during the Preboreal is detected (figure 2(k)). One may speculate that permafrost remained intact in the small Apuka catchment and adjacent shelves until ~11.5 kyr BP.

The mass accumulation rates rapidly culminate in two maxima at ~14.6 and ~11.5 kyr BP (figures 2(i)–(k)). These coincide with mwp-1A and mwp-1B, (figure 2(d)) suggesting that rapid flooding of the Bering Land Bridge and the Pacific shelves adjacent to Siberia and Kamchatka caused massive coastal erosion of permafrost deposits. This is in accordance with the flooding scenario of the Bering Shelf (Manley 2002) which suggests that most of the shelf was flooded between 15 and 10 kyr BP, consistent with high rates of sea-level rise (Lambeck *et al* 2014).

The maxima of massive translocation of permafrost carbon are also synchronous with rapid warming in the North-Pacific realm (Kurek *et al* 2009, Meyer *et al* 2016, 2017, Méheust *et al* 2018) during the onsets of the Bølling-Allerød and Preboreal interstadials (NGRIP 2004) at 14.6 and 11.5 kyr BP. Together with elevated summer insolation (Berger and Loutre 1991) warming may have caused widespread permafrost thaw in the Kamchatka, Apuka, Anadyr and Yukon River watersheds. Subsequent fluvial discharge of the mobilized organic matter may have increased the accumulation of terrigenous biomarkers at our sites. Walter Anthony *et al* (2014) report pronounced expansion of thermokarst lakes in Siberia and Alaska during the interstadials which points to widespread abrupt permafrost thaw across Beringia. Concurrent wetland development in the Anadyr and Yukon catchments—as reported by the increased P_{aq} values (cores SO202-18-3/SO202-18-6, figure 2(h))—suggests generally wetter conditions and possibly amplified overland drainage in Siberia and Alaska. However, the thermokarst-lake expansion peaked during the second half of the warm-spells (figure 2(f)) lagging the abrupt warming and melt-water pulses at 14.6 and 11.5 kyr BP (Reyes and Cooke 2011, Walter Anthony *et al* 2014) as well as the rapid amplification of biomarker accumulation at our sites (figure 2(d), (i)–(k)) at this time. Thus, widespread thaw-induced mobilization of permafrost carbon and subsequent fluvial transport most likely initiated after the melt-water pulses implying that the maxima in accumulation of permafrost carbon at our sites around 14.6 and 11.5 kyr BP (figures 2(i)–(k)) are probably primarily controlled by coastal erosion associated with mwp-1A and mwp-1B. Thaw-induced mobilization of permafrost carbon in the drainage basins of the rivers likely contributed to the elevated mass-accumulation rates of the biomarkers shortly after the melt-water pulses.

Additionally, riverbank erosion of permafrost due to retreating American ice sheets (Keigwin *et al* 2018) and mountain glaciers on Kamchatka (Bigg *et al* 2008) may have proceeded throughout the late deglaciation.

For the Younger Dryas (12.9–11.5 kyr BP), all cores indicate a slackening of the accumulation of terrigenous biomarkers (figures 2(i)–(k)) which coincides with reduced thaw lake development (Walter Anthony *et al* 2014), wetland vegetation (lowered P_{aq} ; cores SO202-18-3/SO202-18-6) and rates of sea-level change. Thus, permafrost decomposition in the interior and along the coast likely weakened, probably in response to cooling in the North Pacific realm (Meyer *et al* 2016, Méheust *et al* 2018) and decelerated sea-level rise (Lambeck *et al* 2014).

All cores display highest mass accumulation rates during the Preboreal indicating that the remobilization of permafrost carbon reached its maximum at this time (figures 2(i)–(k)). Coastal erosion of permafrost may have become maximal during mwp-1B since the flooding scenario for the Bering Shelf shows that mwp-1B inundated a larger area than mwp-1A (Manley 2002). Thermokarst-lake expansion (Walter Anthony *et al* 2014) and wetland extent (P_{aq} ; cores SO202-18-3/SO202-18-6, figures 2(f) and (h)) became maximal (Reyes and Cooke 2011). This observation likely attests to maximal permafrost thaw in Siberia and Alaska considering that during the Preboreal summer insolation and regional temperatures reached the highest values since the LGM (Berger and Loutre 1991, Kurek *et al* 2009, Meyer *et al* 2016).

3.4. The Holocene after 9–0 kyr BP

After the Preboreal (~9–10 kyr BP), all cores display a distinct decrease and subsequent constancy of the mass-accumulation rates of terrigenous biomarkers (figures 2(i)–(k)) suggesting that the remobilization of old permafrost-derived organic carbon diminished and stabilized. Coastal erosion rates likely decreased as the inundation of the Bering Shelf was almost completed around 10 kyr BP (Manley 2002) after the opening of the Bering Strait (~11 kyr BP; Jakobsson *et al* 2017) and mwp-1B (Lambeck *et al* 2014). Thermokarst lake (Walter Anthony *et al* 2014) and wetland formation (P_{aq} cores SO202-18-3/SO202-18-6; figure 2(h)) weakened and stabilized after the Preboreal potentially marking a thorough reduction of inland permafrost thaw and the related discharge of permafrost carbon to our sites (figures 2(i)–(k)).

During the late Holocene, the pre-depositional ages found off Kamchatka (~4500 years; core-top core SO201-2-12KL; figure 2, table 1) are significantly younger than during the deglaciation and the LGM (>6000 years; figure 2(k), table 1). The decrease in age is probably due to the rather limited permafrost extent on Kamchatka at present as most of the peninsula is permafrost free with only a few patches of sporadic and alpine permafrost (Brown *et al* 1998).

3.5. Implications for the carbon cycle

We identify two major intervals of massive land-ocean transfer of old permafrost carbon across Beringia's Pacific coast that occur during the Bølling-Allerød and Preboreal warm-spells. We find that these two intervals initiated rapidly in response to abrupt sea-level rise during mwp-1A and mwp-1B and likely received contributions from thaw-induced processes in the hinterland shortly after the melt-water pulses. Our mass-accumulation rates indirectly mark intervals of enhanced release of ancient CO_2 from degrading permafrost (Winterfeld *et al* 2018) as exposure of previously freeze-locked carbon to microbial activity in the rivers, the marine water column and at the sediment-water interface of the ocean might have resulted in its rapid decomposition.

As such, the centennial-scale amplification of permafrost erosion during mwp-1A and mwp-1B is probably indicative of similarly rapid CO_2 emissions into the atmosphere. Within the uncertainties of the chronologies ($< \pm 300$ years) (Max *et al* 2012, Kuehn *et al* 2014) this rapid carbon release is synchronous with the rapid rises in atmospheric CO_2 at 14.6 and 11.5 kyr BP (Marcott *et al* 2014) (figure 2(b)). The same chronology of processes causing permafrost decomposition as found in our study (coastal erosion followed by inland permafrost thaw and river discharge) has also been inferred from biomarker records from the Okhotsk Sea off the Amur River mouth (Winterfeld *et al* 2018). The consistency implies that at least in the North-Pacific realm sea-level rise was a major control for abrupt remobilization of permafrost carbon at 14.6 and 11.5 kyr BP. As for the Arctic sector of Beringia, deglacial reworking of old permafrost carbon caused by inundation of the Chukchi Shelf (at ~13 kyr BP, figure 2(f)) has been recently reported (Martens *et al* 2019). Yet, it remains unresolved whether Beringia's Arctic shelves (East Siberian Arctic and Chukchi Shelves, figure 1) released carbon at 14.6 and 11.5 kyr BP along with the Pacific shelves (Martens *et al* 2019). Tesi *et al* (2016) document massive fluvial discharge of permafrost carbon from the Lena River into the Laptev Sea around 11.5 kyr BP suggesting that thaw-induced degradation of permafrost in drainage basin of the Lena coincided with rapidly rising atmospheric CO_2 levels (figure 2(f)). Altogether these data confirm model-based hypothesis according to which carbon release from coastal as well as inland permafrost decomposition contributed substantially to the rapid deglacial rises in atmospheric CO_2 (Köhler *et al* 2014, Winterfeld *et al* 2018).

Extrapolating biomarker data from the small Okhotsk-Sea shelves to the extensive Bering, Chukchi and East Siberian Arctic Shelves Winterfeld *et al* (2018) estimated with a carbon cycle model that flooding of this area alone may have accounted for about half of the abrupt rises in atmospheric CO_2 (~6 ppm) at 14.6 and 11.5 kyr BP thereby causing a drop of 6–8‰ in atmospheric $\Delta^{14}\text{C}$. Our data reveal that the timing of

carbon mobilization (peaks in mass-accumulation rates, figures 2(i), (j) and (l)) as well as the pre-depositional ages agree well between the Sea of Okhotsk (~5000–10 000 years; figure 2(l)) and the Bering Sea (~6900–10 500 years; figure 2(i), table 1, cores SO202-18-3/SO202-18-6) at these times. Given these consistencies our findings underpin the results of the carbon cycle simulation by Winterfeld *et al* (2018) highlighting the potential key role of Beringia in the deglacial permafrost-carbon feedback, particularly at 14.6 and 11.5 kyr BP.

At 16.5 kyr BP, flooding of the Bering, Chukchi and East Siberian Arctic Shelves may only explain up to a fourth of the observed sudden rise in atmospheric CO₂ according to Winterfeld *et al* (2018). Our data suggest that next to incipient inundation of the Bering Shelf massive meltwater discharge due to glacier retreat caused riverbank erosion of permafrost soils in the Yukon catchment and concomitantly mobilized fossil, petrogenic carbon around that time (figures 3(a), (d) and (g)). This process could have additionally fueled the observed rise in atmospheric CO₂ at 16.5 kyr BP, if the mobilized material was at least partly remineralized during transport processes prior to final burial in marine sediments and if the melt-water induced mobilization of old carbon was a broad-scale phenomenon around the large Eurasian and American ice sheets.

4. Conclusion

By analyzing mass accumulation rates and pre-depositional ages of terrigenous biomarkers in sediments from the Bering Sea and the Northwest Pacific, we provide the first proxy record constraining mobilization of old carbon during permafrost retreat in Beringia across the entire LGM-Holocene transition. We find that the activation of old, previously freeze-locked carbon rapidly initiated within centennial time-scales matching the rapid increases in atmospheric CO₂ around 16.5, 14.6 and 11.5 kyr BP. The massive remobilization of old terrigenous organic carbon resulted from melt-water runoff, shelf flooding and permafrost thaw in the interior. We infer that, next to warming and subsequent permafrost thaw, rapid shelf flooding during mwp-1A and mwp-1B was an important driver of the enhanced accumulation of permafrost carbon in the N Pacific, particularly during mwp-1A and mwp-1B around 14.6 and 11.5 kyr BP. Our data corroborate recent model-based hypotheses according to which the inundation of the vast East Siberian Arctic, Chukchi and Bering shelves substantially contributed to the sudden rises of atmospheric CO₂ at these times (Winterfeld *et al* 2018). We acknowledge that our data only represent Beringia's Pacific shelves including the Bering Shelf. As the deglacial mobilization of permafrost carbon along the East Siberian Arctic and Chukchi Shelves around

the three rapid shifts in CO₂ is largely unresolved at the present stage (Tesi *et al* 2016, Keskitalo *et al* 2017, Martens *et al* 2019), this hypothesis requires further testing.

Our study reveals that mobilization of petrogenic and permafrost-derived carbon induced by the retreat of continental ice-sheets and associated meltwater floods was a potential mechanism to rapidly unlock ancient terrestrial carbon, a process which has been unrecognized so far (e.g. Köhler *et al* 2014, Lindgren *et al* 2018). The mobilized material may have contributed to rising atmospheric CO₂-levels already during the early deglaciation, potentially explaining parts of the rapid shift at 16.5 kyr BP.

Our study thus emphasizes the general vulnerability of permafrost to abrupt decomposition, in particular the sea-level induced erosion, and the related potential to cause centennial-scale rises in atmospheric CO₂, which might similarly happen in the future.

Acknowledgments

The study is based on core material which was gained in the frame of the German-Russian research project 'KALMAR'—Kurile-Kamchatka and Aleutian Marginal Sea Island Arc Systems: Geodynamic and Climate Interaction in Space and Time' and the 'INOPEX—Innovative North Pacific Experiment' project (BMBF Grant 03G0202A). We thank the Master and the crew of R/V SONNE for their professional support during cruises SO201-2 and SO202. Dirk Nürnberg is acknowledged for providing sample material from site SO201-2-12KL. We thank Arnaud Nicolas, Sara Trojahn and Thorsten Riedel for their valuable assistance on the geochemical sample preparation in the laboratories. The study was funded by the Helmholtz association through the President's Initiative and Networking Fund. It contributes to PALMOD, the German Paleomodelling Research Project funded by the German Federal Ministry for Education and Research (BMBF). We thank two reviewers for their comments and suggestions on earlier version of our manuscript which helped to improve the quality of this article. The biomarker data generated in this study are accessible at the database Pangaea: <https://doi.org/10.1594/PANGAEA.901962>

ORCID iDs

Vera D Meyer  <https://orcid.org/0000-0002-4958-5367>

Jens Hefter  <https://orcid.org/0000-0002-5823-1966>

Peter Köhler  <https://orcid.org/0000-0003-0904-8484>

Ralf Tiedemann  <https://orcid.org/0000-0001-7211-8049>

Gesine Mollenhauer  <https://orcid.org/0000-0001-5138-564X>

References

- AMAP 2012 *Arctic Climate Issues 2011: Changes in Arctic Snow, Water, Ice and Permafrost. SWIPA 2011 Overview Report* (Oslo: Arctic Monitoring and Assessment Programme (AMAP))
- Anderson P M and Lozhkin A V 2015 Late quaternary vegetation of Chukotka (Northeast Russia), implications for glacial and holocene environments of Beringia *Quat. Sci. Rev.* **107** 112–28
- Badding M E, Briner J P and Kaufman D S 2013 ^{10}Be ages of late pleistocene deglaciation and neoglaciation in the north-central Brooks Range Arctic Alaska *J. Quat. Sci.* **28** 95–102
- Balascio N L, Kaufman D S and Manley W F 2005 Equilibrium-line altitudes during the last glacial maximum across the Brooks Range Alaska *J. Quat. Sci.* **20** 821–38
- Barnes F 1967 Coal Resorces of Alaska *Geological Survey Bulletin* 1242-B US Printing Office (<https://doi.org/10.3133/b1242B>)
- Barr I D and Clark C D 2012 Late quaternary glaciations in Far NE Russia; combining moraines, topography and chronology to assess regional and global glaciation synchrony *Quat. Sci. Rev.* **53** 72–87
- Bauska T K, Bagenstos D, Brook E J, Mix A C, Marcott S A, Petrenko V V, Schaefer H, Severinghaus J P and Lee J E 2016 Carbon dioxide isotopes during the deglaciation *Proc. Natl Acad. Soc.* **113** 3465–70
- Berger A and Loutre M F 1991 Insolation values for the climate of the last 10 million years *Quat. Sci. Rev.* **10** 297–317
- Bigg G R, Clark C D and Hughes A L C 2008 A last glacial ice sheet on the Pacific Russian coast and catastrophic change arising from coupled ice-volcanic interaction *Earth Planet. Sci. Lett.* **265** 559–70
- BLM Alaska State Office 2009 Leasable minerals *Mineral Occurrence and Development Potential Report* Division of Energy and Solid Minerals, Branch of Energy pp 1–55
- Bray E and Evans E 1961 Distribution of *n*-paraffins as a clue to recognition of source beds *Geochim. Cosmochim. Acta* **22** 2–15
- Brovkin V, Ganopolski A, Archer D and Munhoven G 2012 Glacial CO_2 cycle as a succession of key physical and biogeochemical processes *Clim. Past* **8** 251–64
- Brown J, Ferrans O J Jr, Heginbottom J A and Melnikov E S 1998 *Circum-Arctic Map of Permafrost and Ground-Ice Conditions* (Boulder, CO: National Snow and Ice Data Center/World Data Center for Glaciology)
- Bröder L, Tesi T, Andersson A, Semiletov I and Gustafsson Ö 2018 Bounding cross-shelf transport time and degradation in Siberian-Arctic land-ocean carbon transfer *Nat. Commun.* **9** 806
- Bröder L, Tesi T, Andersson A, Elington T I, Semiletov I P, Dudarev O V, Roos P and Gustafsson Ö 2016 Historical records of organic matter supply and degradation status in the East Siberian Sea *Org. Geochem.* **91** 16–30
- Bush R T and McInerney F A 2013 Leaf wax *n*-alkane distributions in and across modern plants: implications for paleoecology and chemotaxonomy *Geochim. Cosmochim. Acta* **117** 161–79
- Ciais P *et al* 2012 Large inert carbon pool in the terrestrial biosphere during the last glacial maximum *Nat. Geosci.* **5** 74–9
- Crichton K A, Bouttes N, Roche D M, Chappellaz J and Krinner G 2016 Permafrost carbon as a missing link to explain CO_2 changes during the last deglaciation *Nat. Geosci.* **9** 683–6
- Van Duin A C T, Sinninghe Damsté J S, Koopmans M P, Van De Graaf B and De Leeuw J W 1997 A kinetic calculation method of homohopanoide maturation: applications in the reconstruction of burial histories of sedimentary basins *Geochim. Cosmochim. Acta* **61** 2409–29
- Duk-Rodkin A and Hughes O L 1994 Tertiary-quaternary drainage of the pre-glacial Mackenzie basin *Quat. Int.* **22–23** 221–41
- Dyke A S 2004 An outline of North American deglaciation with emphasis on central and northern Canada *Quat. Glaciations: Extent Chronol.* **2** 373–424
- Eglinton G and Hamilton R J 1967 Leaf epicuticular waxes *Science* **156** 1322–35
- Elias S A 2001 Mutual climatic range reconstructions of seasonal temperatures based on late pleistocene fossil beetle assemblages in Eastern Beringia *Quat. Sci. Rev.* **20** 77–91
- Farrimond P, Taylor A and TelnËs N 1998 Biomarker maturity parameters: the role of generation and thermal degradation *Org. Geochem.* **29** 1181–97
- Feng X, Vonk J E, van Dongen B E, Gustafsson Ö, Semiletov I P, Dudarev O V, Wang Z, Montluçon D B, Wacker L and Eglinton T I 2013 Differential mobilization of terrestrial carbon pools in Eurasian Arctic river basins *Proc. Natl Acad. Sci. USA* **110** 14168–73
- Ficken K J, Li B, Swain D L and Eglinton G 2000 An *n*-alkane proxy for the sedimentary input of submerged/floating freshwater aquatic macrophytes *Org. Geochem.* **31** 745–9
- Gustafsson Ö, Van Dongen B E, Vonk J E, Dudarev O V and Semiletov I P 2011 Widespread release of old carbon across the Siberian arctic echoed by its large rivers *Biogeosciences* **8** 1737–43
- Hopmans E C, Weijers J W, Schefuß E, Herfort L, Sinninghe Damsté J S and Schouten S 2004 A novel proxy for terrestrial organic matter in sediments based on branched and isoprenoid tetraether lipids *Earth Planet. Sci. Lett.* **224** 107–16
- Hugelius G *et al* 2014 Estimated stocks of circumpolar permafrost carbon with quantified uncertainty ranges and identified data gaps *Biogeosciences* **11** 6573–93
- Jakobsson M *et al* 2017 Post-glacial flooding of the Bering land bridge dated to 11 cal ka BP based on new geophysical and sediment records *Clim. Past* **13** 991–1005
- Jones B M *et al* 2018 A decade of remotely sensed observations highlight complex processes linked to coastal permafrost bluff erosion in the Arctic *Environ. Res. Lett.* **13** 115001
- Jongejans L L, Strauss J, Lenz J, Peterse F, Mangelsdorf K, Fuchs M and Grosse G 2018 Organic matter characteristics in yedoma and thermokarst deposits on the Baldwin Peninsula, west Alaska *Biogeosciences* **15** 6033–48
- De Jonge C, Stadnitskaia A, Hopmans E C, Cherkashov G, Fedotov A, Streletskaia I D, Vasiliev A A and Sinninghe Damsté J S 2015 Drastic changes in the distribution of branched tetraether lipids in suspended matter and sediments from the Yenisei River and Kara Sea (Siberia): implications for the use of brGDGT-based proxies in coastal marine sediments *Geochim. Cosmochim. Acta* **165** 200–25
- Keigwin L D, Klotsko S, Zhao N, Reilly B, Giosan L and Driscoll N W 2018 Deglacial floods in the beaufort sea preceded younger dryas cooling *Nat. Geosci.* **11** 599–604
- Kennedy K E, Froese D G, Zazula G D and Lauriol B 2010 Last glacial maximum age for the northwest Laurentide maximum from the eagle river spillway and delta complex, northern Yukon *Quat. Sci. Rev.* **29** 1288–300
- Keskitalo K, Tesi T, Bröder L, Andersson A, Pearce C, Sköld M, Semiletov I P, Dudarev O V and Gustafsson Ö 2017 Sources and characteristics of terrestrial carbon in Holocene-scale sediments of the East siberian sea *Clim. Past* **13** 1213–26
- Kleinen T and Brovkin V 2018 Pathway-dependent fate of permafrost region carbon *Environ. Res. Lett.* **13** 094001
- Köhler P, Fischer H, Munhoven G and Zeebe R E 2005 Quantitative interpretation of atmospheric carbon records over the last glacial termination *Glob. Biogeochem. Cycles* **19** GB4020
- Köhler P, Knorr G and Bard E 2014 Permafrost thawing as a possible source of abrupt carbon release at the onset of the Bølling/Allerød *Nat. Commun.* **5** 5520
- Köhler P, Nehrass-Ahles C, Schmitt J, Stocker T F and Fischer H 2017 A 156 kyr smoothed history of the atmospheric greenhouse gases CO_2 , CH_4 and N_2O and their radiative forcing *Earth Syst. Sci. Data* **9** 363–87

- Koven C D, Ringeval B, Friedlingstein P, Ciais P, Cadule P, Khvorostyanov D, Krinner G and Tarnocai C 2011 Permafrost carbon-climate feedbacks accelerate global warming *Proc. Natl Acad. Sci.* **108** 14769–74
- Kuehn H, Lembke-Jene L, Gersonde R, Esper O, Lamy F, Arz H, Kuhn G and Tiedemann R 2014 Laminated sediments in the Bering Sea reveal atmospheric teleconnections to Greenland climate on millennial to decadal timescales during the last deglaciation *Clim. Past* **10** 2215–36
- Kurek J, Cwynar L C, Ager T A, Abbott M B and Edwards M E 2009 Late quaternary paleoclimate of western Alaska inferred from fossil chironomids and its relation to vegetation histories *Quat. Sci. Rev.* **28** 799–811
- Kusch S, Rethemeyer J, Schefuß E and Mollenhauer G 2010 Controls on the age of vascular plant biomarkers in Black Sea sediments *Geochim. Cosmochim. Acta* **74** 7031–47
- Kvenvolden K A 1966 Molecular distributions of normal fatty acids and paraffins in some lower cretaceous sediments *Nature* **209** 694–6
- Lambeck K, Rouby H, Purcell A, Sun Y and Sambridge M 2014 Sea level and global ice volumes from the last glacial maximum to the Holocene *Proc. Natl Acad. Soc.* **111** 15296–303
- Lindgren A, Hugelius G and Kuhry P 2018 Extensive loss of past permafrost carbon but a net accumulation into present-day soils *Nature* **560** 219–22
- Lindgren A, Hugelius G, Kuhry P, Christensen T R and Vandenberghe J 2015 GIS-based maps and area estimates of northern hemisphere permafrost extent during the last glacial maximum *Permafrost Periglacial Process.* **27** 6–16
- Maier E *et al* 2018 North Pacific freshwater events linked to changes in glacial ocean circulation *Nature* **559** 241–5
- Manley W F 2002 Postglacial flooding of the bering land bridge: a geospatial animation: INSTAAR, University of Colorado, v1 (http://instaar.colorado.edu/QGISL/bering_land_bridge)
- Marcott S A *et al* 2014 Centennial-scale changes in the global carbon cycle during the last deglaciation *Nature* **514** 616–9
- Martens J *et al* 2019 Remobilization of old permafrost carbon to chukchi sea sediments during the end of the last deglaciation *Glob. Biogeochem. Cycles* **33** 2–14
- Max L, Riethdorf J-R, Tiedemann R, Smirnova M, Lembke-Jene L, Fahl K, Nürnberg D, Matul A and Mollenhauer G 2012 Sea surface temperature variability and sea-ice extent in the subarctic northwest Pacific during the past 15,000 years *Paleoceanography* **27** PA3213
- Meyer V D, Hefter J, Lohmann G, Max L, Tiedemann R and Mollenhauer G 2017 Summer temperature evolution on the Kamchatka Peninsula, Russian far east, during the past 20,000 years *Clim. Past* **13** 359–77
- Meyer V D, Max L, Hefter J, Tiedemann R and Mollenhauer G 2016 Glacial-to-Holocene evolution of sea surface temperature and surface circulation in the subarctic northwest Pacific and the Western Bering Sea *Paleoceanography* **31** 916–27
- Méheust M, Stein R, Fahl K and Gersonde R 2018 Sea-ice variability in the subarctic North Pacific and adjacent Bering Sea during the past 25 ka: new insights from IP₂₅ and Uk'₃₇ proxy records *Arktos* **4** 8
- North Greenland Ice Core Project members 2004 High-resolution record of northern hemisphere climate extending into the last inter-glacial period *Nature* **431** 147–51
- Reimer P, Bard E, Bayliss A and Beck J W 2013 IntCal13 and marine13 radiocarbon age calibration curves 0–50,000 years cal BP *Radiocarbon* **55** 1869–87
- Reyes A V and Cooke C A 2011 Northern peatland initiation lagged abrupt increases in deglacial atmospheric CH₄ *Proc. Natl Acad. Sci.* **108** 4748–53
- Schlitzer R 2018 Ocean Data View (<http://odv.awi.de>) (Accessed: 9 September 2018)
- Schuur E A G, McGuire A D, Grosse G, Harden J W, Hayes D J, Hugelius G, Koven C D and Kuhry P 2015 Climate change and the permafrost carbon feedback *Nature* **520** 171–9
- Strauss J *et al* 2017 Deep Yedoma permafrost: a synthesis of depositional characteristics and carbon vulnerability *Earth-Sci. Rev.* **172** 75–86
- Sánchez-García L, Vonk J E, Charkin A N, Kosmach D, Dudarev O V, Semiletov I P and Gustafsson O 2014 Characterisation of three regimes of collapsing arctic ice complex deposits on the SE Laptev Sea coast using biomarkers and dual carbon isotopes *Permafrost Periglacial Process.* **25** 172–83
- Tesi T *et al* 2016 Massive remobilization of permafrost carbon during post-glacial warming *Nat. Commun.* **7** 13653
- Vonk J E and Gustafsson Ö 2013 Permafrost-carbon complexities *Nat. Geosci.* **6** 675–6
- Vonk J E, Semiletov I P, Dudarev O V, Eglinton T I, Andersson A, Shakhova N, Charkin A, Heim B and Gustafsson Ö 2014 Preferential burial of permafrost-derived organic carbon in Siberian-Arctic shelf waters *J. Geophys. Res. Ocean* **119** 8410–21
- Vonk J E *et al* 2012 Activation of old carbon by erosion of coastal and subsea permafrost in Arctic Siberia *Nature* **489** 137–40
- Walter K M, Edwards M E, Grosse G, Zimov S A and Chapin F S III 2007 Thermokarst lakes as a source of atmospheric CH₄ during the last deglaciation *Science* **633** 633–6
- Walter Anthony K M *et al* 2014 A shift of thermokarst lakes from carbon sources to sinks during the Holocene epoch *Nature* **511** 452–6
- Winterfeld M *et al* 2018 Deglacial mobilization of pre-aged terrestrial carbon from degrading permafrost *Nat. Commun.* **9** 3666
- Zazula G D, Duk-Rodkin A, Schweger C E and Morlan R E 2004 Late Pleistocene chronology of glacial lake old crow and the north-west margin of the laurentide ice sheet *Dev. Quat. Sci.* **2** 347–62

Supplementary information

S1. Methods

1. 1. Core material and chronology

Piston-cores SO201-2-114KL and SO201-2-12KL were recovered during cruise RV SONNE SO201 in 2009 (Dullo et al., 2009) within the frame of KALMAR Leg 2. For the record off the Bering Shelf (site SO202-18) a combination of two neighboring cores was used (piston-core SO202-18-3 and kasten-core SO202-18-6). Both were retrieved during cruise RV SONNE SO202 in 2009 (INOPEX; Gersonde (2012)). Integrated age models were developed by accelerator mass spectrometry (AMS) radiocarbon dating of planktonic foraminifera (*Neogloboquadrina pachyderma* sin.) combined with core-to-core correlations of high-resolution spectrophotometric (color b*) and X-ray fluorescence data as well as ash-layers (Max et al., 2012; Kuehn et al., 2014). Max et al. (2012) and Kuehn et al. (2014) converted the radiocarbon ages into calibrated calendar ages using the calibration software Calib Rev 6.0 (Stuiver and Reimer, 1993) with the Intcal09 and Intcal13 atmospheric calibration curves (Reimer et al., 2009; 2013). For cores SO202-18-3 and SO202-18-6, Kuehn et al. (2014) additionally performed a decadal-scale correlation of layer-counted varves and lamination patterns to the NGRIP stable isotope record to determine calendar ages. The 1σ uncertainty of the converted calendar ages from the age-control points for cores SO202-18-3, SO202-18-6, SO201-2-114KL and SO201-2-12KL were smaller than ± 300 years (Max et al., 2012; Kuehn et al., 2014). An important source of uncertainty are changes in reservoir ages of the surface ocean during the last deglaciation (Sarnthein et al., 2015). However, as shown by Kuehn et al. (2014) and Lund et al. (2011) reservoir ages of the Bering Sea and the North Pacific varied by only ~ 300 years over the last deglaciation. Kuehn et al. (2014) used the correlation of laminae structures to the NGRIP record to calculate deglacial reservoir ages in the Bering Sea and found that those ranged between 730 and 1100 years (Kuehn et al., 2014). For the chronologies of cores SO201-2-114KL and SO201-2-12KL Max et al. (2012) assumed a constant reservoir age of 900 years which is well within the range calculated by Kuehn et al. (2014). For more details on the chronologies, the reader is referred to Max et al. (2012) and Kuehn et al. (2014).

Prior to sample preparation, the cores were stored at 4°C. For biomarker quantification and calculation of mass accumulation rates (MAR) the cores were sampled every 10 cm (SO201-2-12KL and SO202-18-3/SO202-18-6) and 5 cm (SO201-2-114KL). Samples for compound-

specific radiocarbon analysis (CSRA) were taken from 5-6 selected horizons (~2cm thickness) in each core.

1. 2. Lipid extraction

Samples were freeze-dried and homogenized with a mortar. Samples determined for calculating biomarker MAR (5g) were extracted by accelerated solvent extraction (Dionex ASE 200) using dichloromethane (DCM):methanol (MeOH) 9:1 (v/v) (22 ml cells, three cycles, 5 minutes each, at 100°C and 1000 psi). Prior to extraction squalane, erucic acid and a C₄₆-GDGT were added as internal standards. Samples for compound-specific radiocarbon analyses (30-80g) were extracted with DCM:MeOH 9:1 (v/v) using a Soxhlet-apparatus (60°C, 48 hours) and were processed without internal standards.

In order to break up wax-esters and to separate acids from neutral compounds, all samples were hydrolyzed with 0.1 N potassium hydroxide (KOH) in MeOH:H₂O 9:1 (v/v) at 80°C for two hours. Neutral compounds were extracted with *n*-hexane, acids with DCM after acidifying the saponified solution with hydrochloric acid (HCL).

Hydrocarbons, including the high molecular weight *n*-alkanes and hopanes, were separated from polar compounds by column-chromatography using deactivated SiO₂. The hydrocarbons were eluted with *n*-hexane, polar compounds with DCM:MeOH 1:1 (v/v). The polar fractions were filtered through 4mm diameter PTFE syringe filters (0.45μm) and were brought to a concentration of 2μg/μl prior to brGDGT analysis. The acid fractions - including the high molecular weight *n*-alkanoic acids, also termed fatty acids (hereafter FA) - were derivatized to methyl esters. The methylation was performed with MeOH of known Δ¹⁴C, together with HCl at 50°C. Air in the headspace of the sample-tube was replaced by nitrogen gas (N₂). Methyl esters were recovered with *n*-hexane and were subsequently cleaned-up with column-chromatography using deactivated SiO₂ and NaSO₄. Methyl esters were eluted with DCM:Hexane 2:1 (v/v).

1. 3. Analysis of FAs and n-alkanes

n-Alkanes and the FA methyl esters (FAMEs) were analyzed using an Agilent7890A gas chromatograph coupled to a flame ionization detector (GC-FID). For technical details see Winterfeld et al. (2018). *n*-Alkanes and FAMEs were identified with an external standard mixture and quantified using the response factors of internal standards (squalane and erucic acid).

Contents of the compounds were normalized to the dry weight of the extracted sediment and total organic carbon (TOC) contents. The standard deviation was determined from repeated measurements of a standard mixture and resulted in an uncertainty of 37% for the contents.

Mass accumulation rates of *n*-alkanes were calculated using the summed contents of the odd carbon numbered homologues (*n*-C₂₃ - *n*-C₃₃). For mass accumulation rates of FAs the saturated even numbered homologues *n*-C_{22:0} - *n*-C_{30:0} were considered.

1. 4. Analysis of homohopane isomers

Hopanes were analyzed using gas chromatography coupled with time of flight mass spectrometry (GC-TOF-MS). The GC-TOF-MS system consisted of a LECO Pegasus III (LECO Corp., St. Joseph, MI) interfaced to an Agilent 6890 GC which was equipped with a temperature programmable cooled injection system (CIS4, Gerstel). The measurements were carried out using the instrumental setup described in Hefter (2008).

Hopanes were identified using relative retention times and mass-spectra. The compounds were quantified using a calibration curve based on 17 β ,21 β (H) hopane (C₃₀ hopane; *m/z* 191). Homohopane isomers (C₃₁) including the 17 β ,21 β (H), 22R homohopane, the 17 β ,21 α (H), 22R + 17 β ,21 α (H), 22S homohopanes (co-elution of the two isomers), the 17 α ,21 β (H), 22R-homohopane and 17 α ,21 β (H), 22S-homohopane were quantified using the sum of: *m/z* 191 + 205. Hopane contents were calculated by normalizing to TOC-contents and to the dry weight of the extracted sediment.

1. 5. Analysis of branched glycerol dialkyl glycerol tetraether (brGDGTs)

brGDGTs were analysed using High Performance Liquid Chromatography/Atmospheric Pressure Chemical Ionization coupled to a single quadrupole mass spectrometer via an Atmospheric Pressure Chemical Ionization interface (HPLC/APCI-MS). Detailed description of the methods applied can be found in Hopmans et al. (2000) and Meyer et al. (2016, 2017). The MS-detector was set in SIM-mode detecting the following (M+H)⁺ ions: *m/z* 1050 (GDGT IIIa), 1048 (GDGT IIIb), 1046 (GDGT IIIc), 1036 (GDGT IIa), 1034 (GDGT IIb), 1032 (GDGT IIc), 1022 (GDGT Ia), 1020 (GDGT Ib), 1018 (GDGT Ic) and 744 (C₄₆-GDGT, internal standard). Contents of brGDGTs were determined using the response factor of the C₄₆-GDGT internal standard and by normalizing to TOC-contents and to the dry weight of the extracted sediment. Due to the lack of appropriate standards, individual relative response factors between the C₄₆-GDGT and the different brGDGTs could not be considered. The obtained contents should be regarded as semi-quantitative. Mass accumulation rates of brGDGTs were determined using the summed contents of GDGT IIIa, GDGT IIIb, GDGT IIIc, GDGT IIa, GDGT IIb, GDGT IIc, GDGT Ia, GDGT Ib and GDGT Ic.

1. 6. Purification of single compounds for CSRA

For CSRA the *n*-alkanes (*n*-C₂₃, *n*-C₂₇ and *n*-C₂₉ alkanes) and the methyl esters of FAs (*n*-C_{26:0} alkanolic acids) were purified using preparative capillary gas chromatography (e.g. Eglinton et al., 1996). We used an Agilent HP6890N gas chromatograph, which was equipped with a temperature programmable cooled injection-system (CIS, Gerstel), and connected to a preparative fraction collector (PFC, Gerstel). More technical details are described in Winterfeld et al. (2018). After isolation the samples were flame-sealed in quartz ampoules on a vacuum line system. The samples were combusted to form CO₂ (950°C) using CuO as oxidizing agent. Afterwards, the gaseous samples were transferred into glass ampoules to prepare them for CSRA.

1.7. CSRA

The isotopic ratio (¹⁴C/¹²C) of the gaseous samples of *n*-alkanes and FAMES was determined by Accelerator Mass Spectrometry (AMS). The measurements were carried out on the MICADAS-system equipped with a gas-ion source (Ruff et al., 2007; Synal et al., 2007; Wacker et al., 2013) at the Institute of Ion Beam Physics, ETH Zurich. AMS-results are reported as “fraction modern carbon” (F¹⁴C) (Stuiver and Pollach, 1977; Reimer et al., 2013). In order to correct for carbon introduced during sample processing, procedure blanks were assessed by isolating FAs from a modern and a fossil standard material according to the methods described above. Apple peel, collected in 2013, was used as modern standard while Messel Shale (an immature Eocene oil Shale from western Germany (Robinson et al., 1989; Abbot et al., 2001)) served as fossil standard. The F¹⁴C and mass of the blank were assessed as in Sun and Meyer et al. (accepted) using a Bayesian approach. Blank-correction of the samples (*n*-alkanes and FAMES) and error propagation was performed after Wacker and Christl (2012). The blank corrected F¹⁴C-values of FAMES were further corrected for the methyl-group, which had been added during the derivatization process, using isotopic mass balance. Using the Intcal13 (Reimer et al., 2013) radiocarbon data were translated into pre-depositional ages (expressed in cal yrs), which describe the age of the compound at the time of deposition (Winterfeld et al. 2018). The time of deposition was inferred from the core chronologies.

1.8. Indicators of thermally mature organic matter

Petrogenic, fossil (¹⁴C-free) organic matter can be distinguished from Yedoma deposits by the state of degradation. Petrogenic organic matter has often undergone severe alteration upon thermal maturation during diagenetic and catagenetic processes (e.g. Kvenvolden et al., 1966; Seifert and Moldowan, 1980; van Duin et al., 1997). By contrast, the frozen conditions in permafrost soils prevent thermal maturation as well as microbial degradation of organic

matter. Studies investigating organic matter in Pleistocene Yedoma and Holocene thermokarst deposits in Siberia and Alaska demonstrate that it is little degraded and does not show any signs of thermal maturation although it is often characterized by low $\Delta^{14}\text{C}$ -values (Sanchez-Garcia et al., 2014; Strauss et al., 2015; Jongejans et al., 2018). In order to assess whether *n*-alkanes and FAs receive significant contributions from petrogenic (thermally altered) organic matter we calculated the carbon preference index of both compound classes (CPI_{alk} , CPI_{FA}). The CPI quantifies the relative abundance of odd- and even-carbon numbered *n*-alkane homologues, and respectively the even-over odd numbered homologues of FAs. The CPI is a common means to estimate the degradation of *n*-alkanes and FA in sediments allowing inferences on thermal maturity (Bray and Evans, 1961; Kvenvolden et al., 1966; Eglinton and Hamilton, 1967). CPI_{alk} -values greater than 3 indicate a predominance of odd carbon numbered homologues which is a typical feature of fresh organic matter in immature deposits (Bray and Evans, 1961; Eglinton and Hamilton, 1967; Bush and McInerney, 2013). Similarly, fresh and immature organic matter found in recent sediments is characterized by an even-over-odd predominance in FAs. Accordingly, CPI-values >3 have been described for *n*-alkanes and FAs in Yedoma and thermokarst deposits in Siberia and Alaska (Sánchez-García et al., 2014; Vonk et al., 2017; Strauss et al., 2015; Jongejans et al., 2018). CPI_{alk} -values near 1 are indicative of thermally altered organic matter as the relative abundance of even-numbered *n*-alkane homologues increases along with thermal maturity (Bray and Evans, 1961; Eglinton and Hamilton, 1967). Similarly, in ancient sedimentary deposits increased relative abundances of odd HMW *n*-alkanoic acids have been described and attributed to diagenetic alteration of organic matter ($\text{CPI}_{\text{FA}} < 2$; Kvenvolden (1966) and references therein).

The CPI-values were calculated as follows:

$$\text{CPI}_{\text{alk}} = 0.5 \left(\frac{(\text{C}_{23} + \text{C}_{25} + \text{C}_{27} + \text{C}_{29} + \text{C}_{31})}{(\text{C}_{22} + \text{C}_{24} + \text{C}_{26} + \text{C}_{28} + \text{C}_{30})} + \frac{(\text{C}_{23} + \text{C}_{25} + \text{C}_{27} + \text{C}_{29} + \text{C}_{31})}{(\text{C}_{23} + \text{C}_{25} + \text{C}_{27} + \text{C}_{29} + \text{C}_{31})} \right)$$

$$\text{CPI}_{\text{FA}} = 0.5 \left(\frac{(\text{C}_{18:0} + \text{C}_{20:0} + \text{C}_{22:0} + \text{C}_{24:0} + \text{C}_{26:0} + \text{C}_{28:0})}{(\text{C}_{17:0} + \text{C}_{19:0} + \text{C}_{21:0} + \text{C}_{23:0} + \text{C}_{25:0} + \text{C}_{27:0})} + \frac{(\text{C}_{18:0} + \text{C}_{20:0} + \text{C}_{22:0} + \text{C}_{24:0} + \text{C}_{26:0} + \text{C}_{28:0})}{(\text{C}_{19:0} + \text{C}_{21:0} + \text{C}_{23:0} + \text{C}_{25:0} + \text{C}_{27:0} + \text{C}_{29:0})} \right)$$

However, it has been found that CPI values show a large variability across modern plant types with mean values ranging between ca. 3-20 (Bush and McInerney, 2013). Moreover, degradation of organic matter during transport prior to final burial in marine sediments (e.g. fluvial or cross-shelf transport) can lower CPI-values (Vonc et al., 2010; Bröder et al., 2016). Variations of CPI in the paleo-record may thus indicate either changes in degradation state,

relative contributions of fossil, petrogenic (thermally altered) organic matter or in plant community (Bush and McInerney, 2013). Therefore, we combine CPI_{alk} and CPI_{FA} with the relative abundances of homohopane isomers (in our case C_{31} -hopanes) to trace contributions of fossil, thermally altered organic matter.

Homohopanes are extended hopanes (C_{31} - C_{35}), which are pentacyclic triterpenoids that are ubiquitous in many geological settings. They are diagenetic products from the bacteriohopanepolyols which are synthesized by bacteria as membrane rigidifiers (e.g. Ensminger et al., 1972; Rohmer et al., 1992). Bacteriohopanepolyols are altered during diagenetic processes including defunctionalisation of the side chains and stereo-isomerization at positions C-17, C-21 and C-22 (Seifert and Moldovan, 1980; Mackenzie and McKenzie, 1983; Rohmer et al., 1992; Sinninghe Damsté et al., 1995; van Duin et al., 1997). The majority of biosynthesized hopanoids possess the $17\beta,21\beta$ (H) 22R stereochemical configuration (Ensminger et al., 1972; Rohmer et al., 1992). As this configuration is thermally unstable the so-called “biologic isomers” are transformed to the $17\beta,21\alpha$ (H) and $17\alpha,21\beta$ (H) stereoisomers (geologic isomers) upon progressing diagenesis and catagenesis (Seifert and Moldovan, 1980; Kolaczowska et al., 1990; Peters and Moldovan, 1993; Sinninghe-Damsté et al., 1995; van Duin et al., 1997; Lockhart et al., 2008). Similarly, with rising temperatures during progressive burial the biologic C-22R configuration is partly turned into its C-22S counterpart generating a mixture of the $17\beta,21\alpha$ (H) 22S, $17\beta,21\alpha$ (H) 22R, $17\alpha,21\beta$ (H) 22S and $17\alpha,21\beta$ (H), 22R epimers (Seifert and Moldovan, 1980; Mackenzie and McKenzie, 1983; van Duin et al., 1997).

While the “diagenetic” $\alpha\beta R$, $\alpha\beta S$, $\beta\alpha R$ and $\beta\alpha S$ isomers are typical of thermally altered deposits and are common in bitumen, kerogen and petroleum the “biologic” $\beta\beta$ -isomers are absent in petroleum and deposits that have undergone early diagenesis which is why they are characteristic of immature, fresh organic matter (e.g. Peters and Moldovan, 1993; Sinninghe-Damsté et al., 1995; Lockhart et al., 2008).

Hence, the relative abundance of “biologic” homohopanes compared to their geologic counterparts in sediments allows qualitative estimates of relative contributions of thermally altered (petrogenic) versus fresh organic matter. We calculated the fractional abundance ($f_{\beta\beta}$) of the $C_{31}\beta\beta R$ homohopane relative to its diagenetic isomers ($C_{31}\alpha\beta R$, $C_{31}\alpha\beta S$, $C_{31}\beta\alpha R$ and $C_{31}\beta\alpha S$) as follows:

$$f_{\beta\beta} = \frac{C_{31}\beta\beta R}{C_{31}\beta\beta R + C_{31}\alpha\beta S + C_{31}\alpha\beta R + C_{31}\beta\alpha S + C_{31}\beta\alpha R}$$

Values of 1 translate to the absence of $\alpha\beta$ and $\beta\alpha$ isomers while 0 indicates the absence of the biologic $\beta\beta$ -isomer. Thus, the smaller the value the greater the portion of degraded, mature organic matter. In some cases, the formation of the $C_{31}\alpha\beta R$ isomer has been observed in thermally immature deposits (mainly peat) where it is attributed to degradation of $C_{31}\beta\beta R$ homohopane under acidic conditions (Inglis et al., 2018 and refs. therein). Significant input from peat deposits to our sediment cores may lower the $f\beta\beta$ accordingly and could be erroneously interpreted as a petrogenic fingerprint. However, peat deposits possessing high relative abundances of the $C_{31}\alpha\beta R$ epimer (and low $f\beta\beta$, respectively), only contain very small traces of the $C_{31}\alpha\beta S$ counterpart (Inglis et al., 2018). By contrast, thermally altered organic matter (e.g. kerogen) is generally characterized by high relative abundances of the 22S epimers that often equal or exceed the abundance of the 22R isomers (e.g. van Duin et al., 1997; Lockhart et al., 2008). In order to avoid a bias stemming from the erosion of peat deposits, we present the $f\beta\beta$ along with the contents of the single isomers (Figure S1).

1.9. Wetland vegetation

It was found that *n*-alkane distributions from peat bogs as well as submerged freshwater plants in lakes are dominated by the *n*-C₂₃ and *n*-C₂₅ homologues while subaerial terrestrial higher plants predominantly synthesize *n*-C₂₇, *n*-C₂₉ and *n*-C₃₁ (Ficken et al., 2000, Vonk and Gustafsson, 2009). Thus, Ficken et al. (2000) introduced the P_{aq} as indicator for the relative abundance of aquatic to terrestrial plants. The index has been commonly applied to trace wetland vegetation in the catchments of marine sediment cores (e.g. Seki et al., 2012).

$$P_{aq} = \frac{C_{23} + C_{25}}{C_{23} + C_{25} + C_{29} + C_{31}}$$

Since wetland development occurs concomitantly to permafrost thaw (AMAP, 2012) we use P_{aq} as proxy for vegetation changes associated with thaw-induced permafrost degradation in the hinterland of our cores.

S2. Tables and figures

Table S1. CSRA raw data of fatty acids (*n*-C_{26:0}) and *n*-alkanes (*n*-C₂₃, *n*-C₂₇, *n*-C₂₉) for cores SO202-18-6, SO20218-3, SO201-2-114KL and SO201-2-12KL. The data were generated using the MICADAS at ETH Zurich.

| Sample depth [cm b.s.f.] | compound | F ¹⁴ C ± σF ¹⁴ C | Sample size [μg C] | ETH ID number |
|-----------------------------|-----------------------------|--|--------------------------|------------------|
| SO202-18-6 | | | | |
| 55-57 | <i>n</i> -C _{26:0} | 0.2046 ± 0.0034 | 111 | 74365.1.1 |
| 200-202 ^{1a} | <i>n</i> -C _{26:0} | 0.1359 ± 0.0029 | 149 | 74364.1.2 |
| 200-202 ^{1b} | <i>n</i> -C _{26:0} | 0.1639 ± 0.0026 | 72 | 74364.1.1 |
| 460-462 ^{1a} | <i>n</i> -C _{26:0} | 0.1265 ± 0.0024 | 130 | 74360.1.2 |
| 460-462 ^{1b} | <i>n</i> -C _{26:0} | 0.1847 ± 0.0027 | 68 | 74360.1.1 |
| SO202-18-3 | | | | |
| 739-742 | <i>n</i> -C _{26:0} | 0.1265 ± 0.0021 | 70 | 74357.1.1 |
| 995-997 | <i>n</i> -C _{26:0} | 0.0918 ± 0.0016 | 146 | 74356.1.1 |
| 1146-1149 ^{1a} | <i>n</i> -C _{26:0} | 0.0580 ± 0.0012 | 117 | 74349.1.2 |
| 1146-1149 ^{1b} | <i>n</i> -C _{26:0} | 0.0850 ± 0.0021 | 58 | 74349.1.1 |
| SO201-2-114KL | | | | |
| 39-41.5 | <i>n</i> -C _{26:0} | 0.1092 ± 0.0026 | 152.2 | 59314.1.1 |
| 101-103.5 | <i>n</i> -C _{26:0} | 0.1136 ± 0.0028 | 83.5 | 59315.1.1 |
| 144-146.5 | <i>n</i> -C _{26:0} | 0.0983 ± 0.0029 | 98.3 | 59318.1.1 |
| 144-146.5 | <i>n</i> -C ₂₇ | 0.179 ± 0.0023 | 42 | 74359.1.1 |
| 144-146.5 | <i>n</i> -C ₂₃ | 0.2173 ± 0.0030 | 25 | 74358.1.1 |
| 174-176.5 | <i>n</i> -C _{26:0} | 0.0926 ± 0.0027 | 74.3 | 59317.1.1 |
| 174-176.5 | <i>n</i> -C ₂₉ | 0.1300 ± 0.0021 | 50 | 74353.1.1 |
| 174-176.5 | <i>n</i> -C ₂₇ | 0.0974 ± 0.0017 | 57 | 74354.1.1 |
| 174-176.5 | <i>n</i> -C ₂₃ | 0.0933 ± 0.019 | 51 | 74355.1.1 |
| 301-303.5 | <i>n</i> -C _{26:0} | 0.0404 ± 0.0025 | 51.7 | 59316.1.1 |
| 301-303.5 | <i>n</i> -C ₂₉ | 0.1072 ± 0.0020 | 40 | 74351.1.1 |
| 301-303.5 | <i>n</i> -C ₂₇ | 0.0976 ± 0.0017 | 37 | 74350.1.1 |
| 301-303.5 | <i>n</i> -C ₂₃ | 0.1840 ± 0.0030 | 21 | 74352.1.1 |
| SO201-2-12KL | | | | |
| 1-4.5 | <i>n</i> -C _{26:0} | 0.5730 ± 0.0074 | 17.6 | 59320.1.1 |
| 203-205 | <i>n</i> -C _{26:0} | 0.1636 ± 0.0029 | 100.2 | 59313.1.1 |
| 295-297 | <i>n</i> -C _{26:0} | 0.3232 ± 0.0064 | 13.9 | 59337.1.1 |
| 419-422 | <i>n</i> -C _{26:0} | 0.1228 ± 0.0028 | 72.3 | 59309.1.1 |
| 609-612 | <i>n</i> -C _{26:0} | 0.1214 ± 0.0030 | 46.4 | 59308.1.1 |
| 693-696 | <i>n</i> -C _{26:0} | 0.0858 ± 0.0026 | 71.2 | 59312.1.1 |
| 896-898 | <i>n</i> -C _{26:0} | 0.0847 ± 0.0029 | 36.9 | 59321.1.1 |

¹ split up for vacuum-line handling in order to keep the sample size (i.e. gas volume) appropriate for the MICADAS. ^a 70%-split, ^b 30%-split.

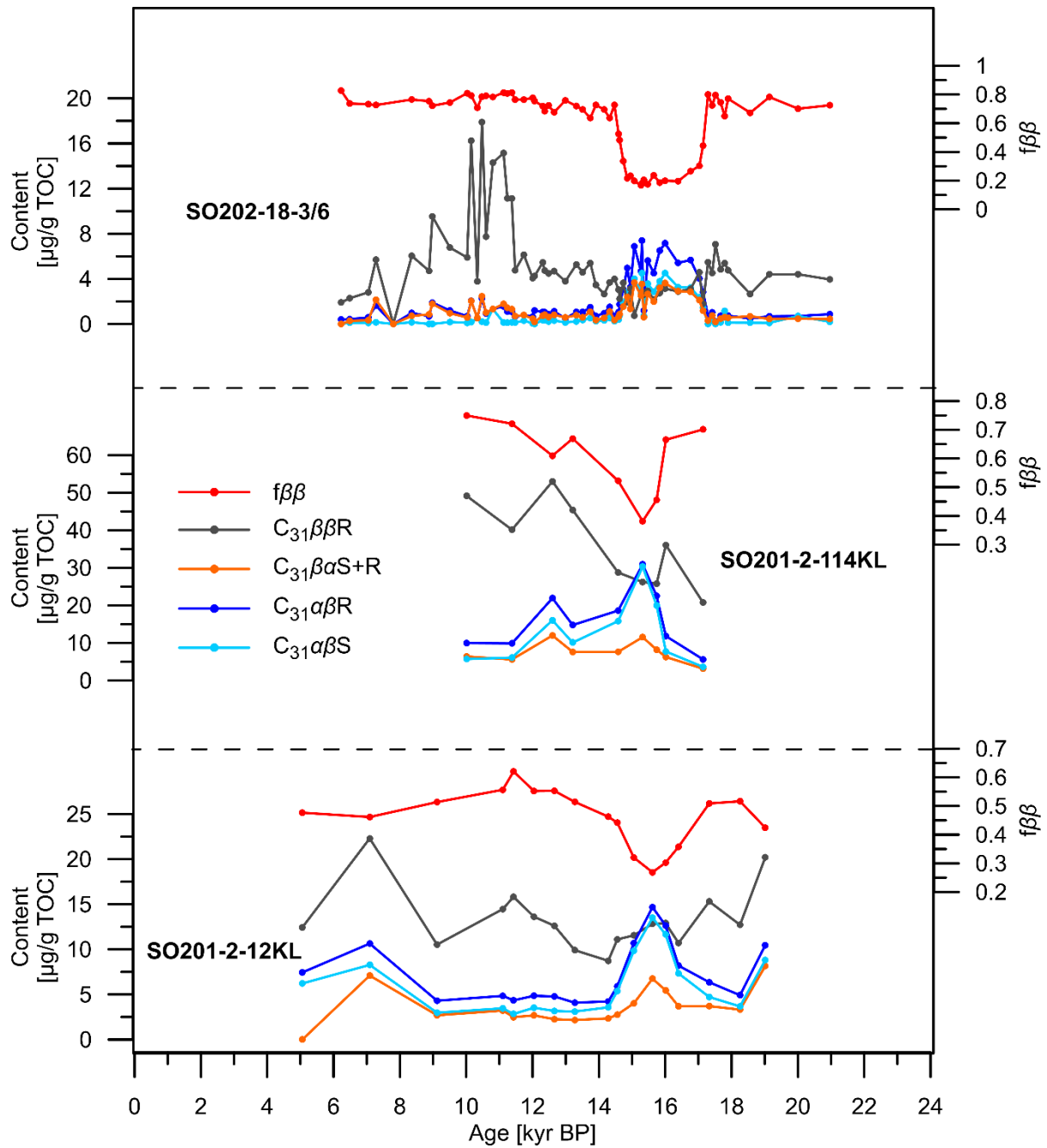


Figure S1: $f_{\beta\beta}$ and the contents of the different C_{31} -homohopane isomers for cores SO202-18-3/SO202-18-6, SO201-2-114KL and SO201-2-12KL. $C_{31}\beta\alpha S$ and $C_{31}\beta\alpha R$ are combined due to co-elution on the GC-MS system.

References

Abbott G D, Zahra Bashir F and Sugden M A 2001 Kerogen-bound and free hopanoic acids in the messel oil shale kerogen *Chirality* **13** 510–516, <http://doi.org/10.1002/chir.1069>

AMAP, 2012. Arctic Climate Issues 2011: Changes in Arctic Snow, Water, Ice and Permafrost. SWIPA 2011 Overview Report. Arctic Monitoring and Assessment Programme (AMAP), Oslo.

- Bray E and Evans E 1961 Distribution of *n*-paraffins as a clue to recognition of source beds. *Geochim. Cosmochim. Acta* **22** 2–15
- Bröder L, Tesi T, Andersson A, Eglinton T I, Semiletov I P, Dudarev O V, Roos P and Gustafsson Ö 2016 Historical records of organic matter supply and degradation status in the East Siberian Sea *Org. Geochem.* **91** 16–30, doi: 0.1016/j.orggeochem.2015.10.008
- Bush R T and McInerney F A. 2013 Leaf wax *n*-alkane distributions in and across modern plants: Implications for paleoecology and chemotaxonomy *Geochim. Cosmochim. Acta* **117** 161–79, doi:10.1016/j.gca.2013.04.016
- Dullo W C, Baranov B and van den Bogaard C 2009 FS Sonne Fahrtbericht/Cruise Report SO201–2 *IFM-GEOMAR, Kiel, Rep.* **35**, IFM262 GEOMAR
- Eglinton T I, Aluwihare L I, Bauer J E, Druffel E R M and McNichol A P 1996 Gas Chromatographic Isolation of Individual Compounds from Complex Matrices for Radiocarbon Dating *Anal. Chem.* **68** 904–912
- Eglinton G and Hamilton R J 1967 Leaf epicuticular waxes *Science* **156** 1322–1334
- Ensminger A, Albrecht P, Ourisson G, Kimble B J, Maxwell J R and Eglinton G 1972 Homohopane in Messel oil shale: first identification of a C₃₁ pentacyclic triterpane in nature *Tetrahedron Letters* **13** 3861–3864
- Ficken K J, Li B, Swain D L and Eglinton G 2000 An *n*-alkane proxy for the sedimentary input of submerged/floating freshwater aquatic macrophytes *Org. Geochem.* **31** 745–9, doi:10.1016/S0146-6380(00)00081-4
- Gersonde, R 2012 The Expedition of the Research Vessel “Sonne” to the Subpolar North Pacific and the Bering Sea in 2009 (SO202- INOPEX) in: *Report on Polar and Marine Research* **643**, edited by: Gersonde R., Alfred Wegener Institute for Polar and Marine Research, Bremerhaven
- Hefter, J 2008 Analysis of Alkenone Unsaturation Indices with Fast Gas Chromatography/Time-of-Flight Mass Spectrometry *Anal. Chem.* **80** 2161–70, <http://doi.wiley.com/10.1029/2001GC000159>
- Hopmans E C, Schouten S, Pancost R D, Van Der Meer M T J and Sinninghe Damsté, J S 2000 Analysis of intact tetraether lipids in archaeal cell material and sediments by high performance liquid chromatography/atmospheric pressure chemical ionization mass spectrometry *Rapid communications in mass spectrometry* **14** 585–9
- Inglis G N, Naafs B D A, Zheng Y, McClymont E L, Evershed R P and Pancost R D 2018 Distributions of geohopanooids in peat: Implications for the use of hopanooid-based proxies in natural archives *Geochim. Cosmochim. Acta* **224** 249–61, <https://doi.org/10.1016/j.gca.2017.12.029>
- Jongejans L L, Strauss J, Lenz J, Peterse F, Mangelsdorf K, Fuchs M and Grosse G 2018 Organic matter characteristics in yedoma and thermokarst deposits on Baldwin Peninsula, west Alaska *Biogeosciences* **15** 6033–48, doi: 10.5194/bg-15-6033-2018

- Kolaczowska E, Slougui N-E, Watt D S, Maruca R E, and Moldowan J M 1990 Thermodynamic stability of various alkylated, dealkylated and rearranged 17 α - and 17/ β -hopane isomers, using molecular mechanics calculations *Org. Geochem.* **16** 1033-1038
- Kuehn H, Lembke-Jene L, Gersonde R, Esper O, Lamy F, Arz H, Kuhn G and Tiedemann R 2014 Laminated sediments in the Bering Sea reveal atmospheric teleconnections to Greenland climate on millennial to decadal timescales during the last deglaciation *Clim. Past* **10** 2215–36, doi: 10.5194/cp-10-2215-2014
- Kvenvolden K A 1966 Molecular Distributions of Normal Fatty Acids and Paraffins in some lower Cretaceous Sediments *Nature* **209** 694–6, doi: 10.1038/209573a0
- Lockhart R S, Meredith W, Love G D and Snape C E 2008 Release of bound aliphatic biomarkers via hydropyrolysis from Type II kerogen at high maturity *Org. Geochem.* **39** 1119–24, doi: 10.1016/j.orggeochem.2008.03.016
- Lund D C, Mix A C and Southon J 2011 Increased ventilation age of the deep northeast Pacific Ocean during the last deglaciation *Nat. Geosci.* **4** 771–774, doi:10.1038/ngeo1272
- Mackenzie A S and McKenzie D 1983 Isomerization and aromatization of hydrocarbons in sedimentary basins formed by extension *Geol. Mag.* **120** 417-528
- Max L, Riethdorf J-R, Tiedemann R, Smirnova M, Lembke-Jene L, Fahl K, Nürnberg D, Matul A and Mollenhauer G 2012 Sea surface temperature variability and sea-ice extent in the subarctic northwest Pacific during the past 15,000 years *Paleoceanography* **27** PA3213, doi:10.1029/2012PA002292
- Meyer V D, Hefter J, Lohmann G, Max L, Tiedemann R and Mollenhauer G 2017 Summer temperature evolution on the Kamchatka Peninsula, Russian Far East, during the past 20,000 years *Clim. Past* **13** 359–77, doi:10.5194/cp-13-359-2017
- Meyer V D, Max L, Hefter J, Tiedemann R and Mollenhauer G 2016 Glacial-to-Holocene evolution of sea surface temperature and surface circulation in the subarctic northwest Pacific and the Western Bering Sea *Paleoceanography* **31** 916–27, doi: 10.1002/2015PA002877
- North Greenland Ice Core Project members 2004 High-resolution record of northern hemisphere climate extending into the last inter- glacial period *Nature* **431** 147–151, doi:10.1038/nature02805
- Peters, K E and Moldowan, J M 1993 *The Biomarker Guide Prentice HaH, Englewood Cliffs, New Jersey*
- Reimer P, Bard E, Bayliss A and Beck J W 2013 IntCal13 and Marine13 Radiocarbon Age Calibration Curves 0–50,000 Years cal BP *Radiocarbon* **55** 1869–87, doi: 10.2458/azu_js_rc.55.16947
- Reimer P J, Baillie M G, Bard E, Bayliss A, Beck J W, Blackwell P G, Bronk Ramsey C, Buck C E, Burr G S, Edwards R L, Friedrich M, Grootes P M, Guilderson T P, Hajdas I, Heaton T J, Hogg A G, Hughen K A, Kaiser K F, Kromer B, McCormac F G, Manning S

- W, Reimer R W, Richards D A, Southon J R, Talamo S, Turney C S M, van der Plicht J and Weyhenmeyer C E 2009 Intcal09 and marine09 radiocarbon age calibration curves, 0–50,000 years cal BP *Radiocarbon* **51** 1111–1150, <https://doi.org/10.1017/S0033822200034202>
- Robinson N, Eglinton G, Cranwell P A, and Zeng Y B 1989 Messel oil shale (western Germany): Assessment of depositional palaeoenvironment from the content of biological marker compounds *Chemical Geology* **76** 153–173, [http://doi.org/10.1016/0009-2541\(89\)90134-4](http://doi.org/10.1016/0009-2541(89)90134-4)
- Rohmer M, Bisseret P and Neunlist S. 1992 The hopanoids, prokaryotic triterpenoids and precursors of ubiquitous molecular fossils *In Biological Markers in Sediments and Petroleum (ed. J. M. Moldowan et al.)*, pp. 1- 17. Prentice Hall
- Ruff M, Wacker L, Gäggeler H W, Suter M, Synal H A and Szidat S 2007 A Gas Ion Source for Radiocarbon Measurements at 200 kV. *Radiocarbon* **49** 307-314
- Sánchez-García L, Vonk J E, Charkin A N, Kosmach D, Dudarev O V, Semiletov I P and Gustafsson O 2014 Characterisation of three regimes of collapsing arctic ice complex deposits on the SE Laptev Sea coast using biomarkers and dual carbon isotopes *Permafrost. Periglac. Process.* **25** 172–83, doi: 10.1002/ppp.1815
- Sarnthein M, Balmer S, Grootes P M and Mudelsee M 2015 Planktic and Benthic ¹⁴C Reservoir Ages for Three Ocean Basins, Calibrated by a Suite of ¹⁴C Plateaus in the Glacial-to-Deglacial Suigetsu Atmospheric ¹⁴C record *Radiocarbon* **57** 129–51, https://doi.org/10.2458/azu_rc.57.17916
- Seifert W K and Moldowan J M 1980 The effect of thermal stress on source rock quality as measured by hopane stereochemistry *Phys. Chem. Earth* **12** 229-237.
- Seki O, Harada N, Sato M, Kawamura K, Ijiri A and Nakatsuka T 2012 Assessment for paleoclimatic utility of terrestrial biomarker records in the Okhotsk Sea sediments *Deep. Res. Part II Top. Stud. Oceanogr.* **61–64** 85–92 <http://dx.doi.org/10.1016/j.dsr2.2011.03.008>
- Sinninghe Damsté J S, Van Duin A C T, Hollander D, Kohnen M E L and De Leeuw J W 1995 Early diagenesis of bacteriohopanepolyol derivatives: Formation of fossil homohopanoids *Geochim. Cosmochim. Acta* **59** 5141–57, doi: 10.1016/0016-7037(95)00338-X
- Strauss J, Schirrmeister L, Mangelsdorf K, Eichhorn L, Wetterich S and Herzschuh U 2015 Organic-matter quality of deep permafrost carbon - A study from Arctic Siberia *Biogeosciences* **12** 2227–45, doi: 10.5194/bg-12-2227-2015
- Stuiver M and Reimer P J 1993 Extended C-14 Data-Base and Revised Calib 3.0 C-14 Age Calibration Program *Radiocarbon* **35** 215–230
- Stuiver M and Polach H A 1977 Reporting of ¹⁴C Data *Radiocarbon* **19** 355-363
- Sun S, Meyer V D, Dolman A D, Winterfeld M, Hefter J, Dummann W, McIntyre C, Montluçon D B, Haghipour N, Wacker L, Gentz T, van der Voort T S, Eglinton T I and

- Mollenhauer G 2019 ^{14}C blank assessment in small-scale compound-specific radiocarbon analysis of lipid biomarkers and lignin phenols *Radiocarbon* **accepted**
- Synal H-A, Stocker M and Suter M 2007 MICADAS: A new compact radiocarbon AMS system *Nuclear Inst Meth* **259** 7–13
- Wacker L and Christl M 2012 Data reduction for small samples. Error propagation using the model of constant contamination *Annual Report of Ion Beam Physics, ETH Zürich* **36**
- Wacker L et al. 2013 A versatile gas interface for routine radiocarbon analysis with a gas ion source *Nuclear Inst Meth* **294** 315–319.
- Winterfeld M, Mollenhauer G, Dummann W, Köhler P, Lembke-Jene L, Meyer V D, Hefter J, McIntyer C, Wacker L, Kokfelt U and Tiedemann R 2018 Deglacial mobilization of pre-aged terrestrial carbon from degrading permafrost *Nat. Comm.* **9** 3666, doi: 10.1038/s41467-018-06080-w
- Van Duin A C T, Sinninghe Damsté J S, Koopmans M P, Van De Graaf B and De Leeuw J W 1997 A kinetic calculation method of homohopanoide maturation: Applications in the reconstruction of burial histories of sedimentary basins *Geochim. Cosmochim. Acta* **61** 2409–29, doi: 10.1016/S0016-7037(97)00105-1
- Vonk J E and Gustafsson Ö 2009 Calibrating *n*-alkane Sphagnum proxies in sub-Arctic Scandinavia *Org. Geochem.* **40** 1085–90, doi: 10.1016/j.orggeochem.2009.07.002
- Vonk J E, Sánchez-García L, Semiletov I, Dudarev O, Eglinton T, Andersson A and Gustafsson O 2010 Molecular and radiocarbon constraints on sources and degradation of terrestrial organic carbon along the Kolyma paleoriver transect, East Siberian Sea *Biogeosciences* **7** 3153–66, doi: 10.5194/bg-7-3153-2010
- Vonk J E, Tesi T, Bröder L, Holmstrand H, Hugelius G, Andersson A, Dudarev O, Semiletov I and Gustafsson Ö 2017 Distinguishing between old and modern permafrost sources in the northeast Siberian land-shelf system with compound-specific $\delta^2\text{H}$ analysis *Cryosphere* **11** 1879–95, doi: 10.5194/tc-11-1879-2017